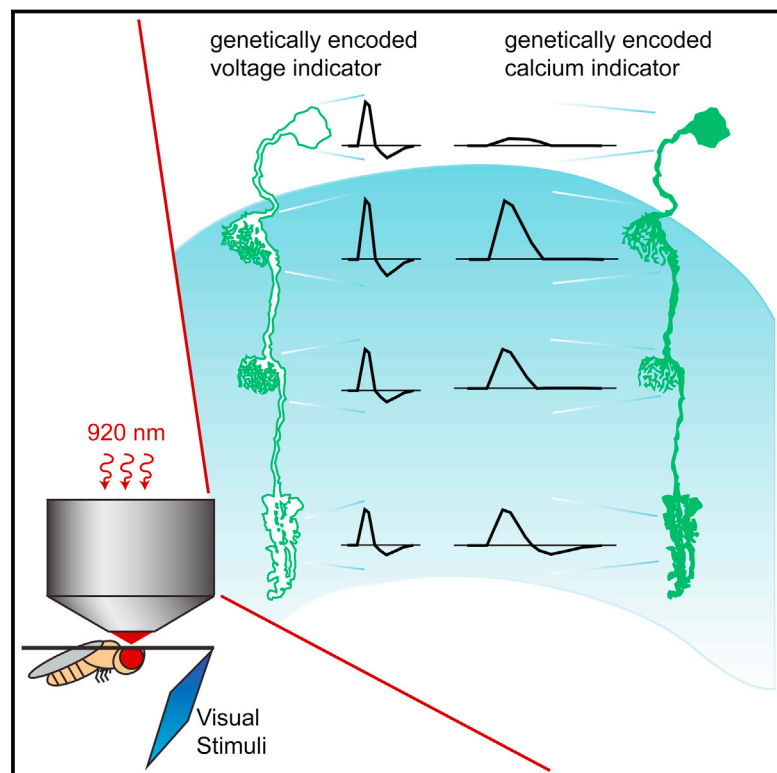


Subcellular Imaging of Voltage and Calcium Signals Reveals Neural Processing In Vivo

Graphical Abstract



Authors

Helen H. Yang, François St-Pierre, Xulu Sun, Xiaozhe Ding, Michael Z. Lin, Thomas R. Clandinin

Correspondence

trc@stanford.edu

In Brief

Observation of subcellular changes in membrane potential and calcium concentration using two-photon imaging of genetically encoded indicators illuminates neuronal computations in vivo, including the origin of ON and OFF selectivity.

Highlights

- In vivo, two-photon imaging of novel genetically encoded voltage indicators
- Observing sensory stimulus-evoked voltage signals with subcellular resolution
- Calcium signals, unlike voltage signals, are compartmentalized within a neuron
- ON and OFF selectivity arises in the transformation between voltage and calcium



Subcellular Imaging of Voltage and Calcium Signals Reveals Neural Processing In Vivo

Helen H. Yang,^{1,3} François St-Pierre,^{2,3,4,5} Xulu Sun,¹ Xiaozhe Ding,² Michael Z. Lin,^{1,2} and Thomas R. Clandinin^{1,*}

¹Department of Neurobiology, Stanford University, Stanford, CA 94305, USA

²Department of Bioengineering, Stanford University, Stanford, CA 94305, USA

³Co-first author

⁴Present address: Department of Neuroscience, Baylor College of Medicine, Houston, TX 77030, USA

⁵Present address: Department of Electrical and Computer Engineering, Rice University, Houston, TX 77005, USA

*Correspondence: trc@stanford.edu

<http://dx.doi.org/10.1016/j.cell.2016.05.031>

SUMMARY

A mechanistic understanding of neural computation requires determining how information is processed as it passes through neurons and across synapses. However, it has been challenging to measure membrane potential changes in axons and dendrites in vivo. We use in vivo, two-photon imaging of novel genetically encoded voltage indicators, as well as calcium imaging, to measure sensory stimulus-evoked signals in the *Drosophila* visual system with subcellular resolution. Across synapses, we find major transformations in the kinetics, amplitude, and sign of voltage responses to light. We also describe distinct relationships between voltage and calcium signals in different neuronal compartments, a substrate for local computation. Finally, we demonstrate that ON and OFF selectivity, a key feature of visual processing across species, emerges through the transformation of membrane potential into intracellular calcium concentration. By imaging voltage and calcium signals to map information flow with subcellular resolution, we illuminate where and how critical computations arise.

INTRODUCTION

Neuronal circuits perform a diverse array of computations to ultimately guide animal behavior. These circuits encode information in dynamic changes in neuronal membrane potential and intracellular calcium concentration; stepwise transformations of these signals then provide the mechanistic basis for extracting behaviorally relevant features. Thus, mapping these signals as they flow along dendrites and axons and across synapses is critical to understanding neural processing. Here, we describe a broadly applicable approach for measuring voltage and calcium changes with subcellular resolution in vivo.

Sensory systems link critical information from the environment to behavior. Given their experimental tractability, these systems have long been studied to understand neural computation, and the information extracted by many peripheral sensory circuits

has been characterized in detail. For example, in many sensory systems, including vision, chemosensation, audition, and thermosensation, a single input is initially transformed into two representations, an ON pathway for increases in signal intensity and an OFF pathway for decreases (Chalasani et al., 2007; Kuffler, 1953; Liu et al., 2015; Scholl et al., 2010; Wässle, 2004). This fundamental organizational principle has been associated with a variety of different strategies for efficiently extracting information about the natural world (Clark et al., 2014; Gjorgjieva et al., 2014; Westheimer, 2007). Thus, understanding where and how circuits implement ON and OFF selectivity provides fundamental insights into neuronal computation.

The *Drosophila* visual system represents a powerful in vivo model for exploring the mechanistic basis of neuronal computation. Experimentally, cell-type-specific expression of genetically encoded indicators of neural activity is straightforward, the optic lobes are accessible for live imaging, well-controlled stimuli can be presented, the cell types are well-defined, and their synaptic connections have been reconstructed at the ultrastructural level (Borst, 2014; Sillescu et al., 2014). Biologically, the fly visual system performs computations essential for behavior using algorithms that are broadly conserved across visual systems. For example, like the vertebrate visual system (Wässle, 2004), the *Drosophila* visual system is split into ON and OFF pathways (Clark et al., 2011; Joesch et al., 2010; Maisak et al., 2013). The lamina monopolar cells L1 and L2 are the strongest synaptic targets of R1–R6 photoreceptors in the lamina and provide input into ON circuitry for light increments and OFF circuitry for light decrements, respectively, in the medulla (Figure 1A). L1 makes synapses onto Mi1 and Tm3; L2 makes synapses onto Tm1 and Tm2 (Takemura et al., 2013). Synapsing in the medulla and the lobula, these medulla interneurons then provide input onto deeper circuitry, including the direction selective cells T4 and T5 (Shinomiyama et al., 2014; Takemura et al., 2013), and represent central feedforward visual pathways.

Mapping transformations of visual information onto changes in membrane potential in dendrites and axons critically depends on a genetically encoded voltage indicator that can capture signals in vivo. Here, we describe fast, bright, two-photon compatible voltage indicators that capture responses predicted from biophysical neuronal models and previously reported electrophysiological measurements. Using these indicators as well as genetically encoded calcium indicators, we reveal the local changes in

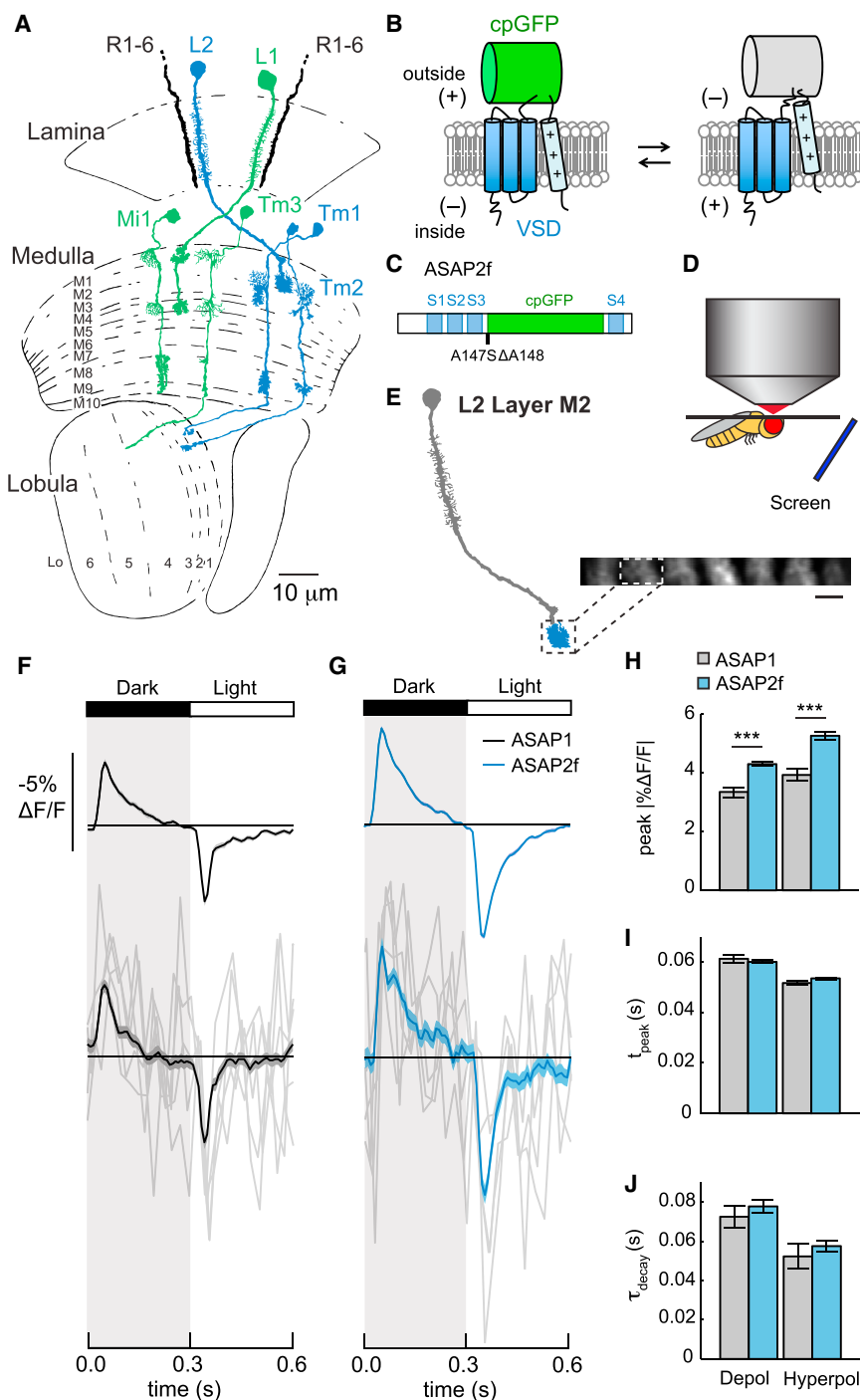


Figure 1. Voltage Imaging in the *Drosophila* Visual System

(A) The *Drosophila* visual system. L1 and L2 receive input from photoreceptors R1–R6 in the lamina neuropil. L1 synapses onto Mi1 and Tm3 in layers M1 and M5 of the medulla neuropil. L2 synapses onto Tm1 and Tm2 in medulla layer M2. L1 and its postsynaptic partners are in green; L2 and its postsynaptic partners are in blue. Tm1, Tm2, and Tm3 project axons into the lobula neuropil. In all figures, cell diagrams modified from Fischbach and Dittrich (1989).

(B) In ASAP sensors, changes in membrane potential induce movement of a positively charged transmembrane helix of a voltage-sensitive domain (VSD), altering the fluorescence of a circularly permuted GFP (cpGFP).

(C) Schematic diagram of ASAP2f, showing the VSD transmembrane domains (S1–S4, blue), cpGFP (green), and the location of the residues changed from ASAP1 (A147S Δ A148).

(D) Schematic illustration of the setup for in vivo, two-photon imaging of visually evoked responses in *Drosophila*.

(E) Illustration of L2 with the imaged region, the axon terminal in medulla layer M2, highlighted. Inset: in vivo, two-photon image of L2 axon terminals expressing ASAP2f, averaged across one time series. One axon terminal is highlighted. Scale bar, 5 μm .

(F and G) Responses of L2 neurons to alternating 300 ms-long dark and light flashes, as measured with (F) ASAP1 ($n = 52$ cells, 3 flies) and (G) ASAP2f ($n = 170$ cells, 8 flies). Top: mean response across all cells. Each cell contributes its average response across 100 trials (1 trial = 1 dark flash and 1 light flash). Bottom: five exemplar single-trial responses from a representative L2 cell (gray) and the same cell's mean response averaged over all trials (black or blue). The solid line is the mean response; the shading is ± 1 SEM.

(H–J) Parameters quantifying the response: (H) peak $\Delta F/F$; (I) t_{peak} ; (J) τ_{decay} . The mean ± 1 SEM is plotted. *** $p < 0.001$ (two-sample t test, Bonferroni correction for multiple comparisons).

See also Figures S1 and S2 and Table S1.

voltage and calcium signaling that transform sensory information in the *Drosophila* visual system.

RESULTS

Benchmarking In Vivo Voltage Imaging of ASAP2f

We began our study of information processing in the visual system by developing a genetically encoded voltage sensor with

higher sensitivity and rapid kinetics that is compatible with two-photon imaging in the fly. We chose the voltage sensor ASAP1 as our starting point for further engineering (St-Pierre et al., 2014). In this indicator, a circularly permuted GFP (cpGFP) is inserted into a voltage-sensing domain (VSD) from a voltage-sensitive phosphatase (Figure 1B). Voltage-induced conformational changes in the VSD perturb GFP fluorescence, such that depolarizations decrease GFP fluorescence and hyperpolarizations increase it. These responses have fast on and off time constants of ~ 2.5 ms (Table S1) (St-Pierre et al., 2014). Based on in vitro characterization of variants with mutations in the linker between the third transmembrane segment of the VSD (S3) and GFP (Figures S1 and S2A–S2C;

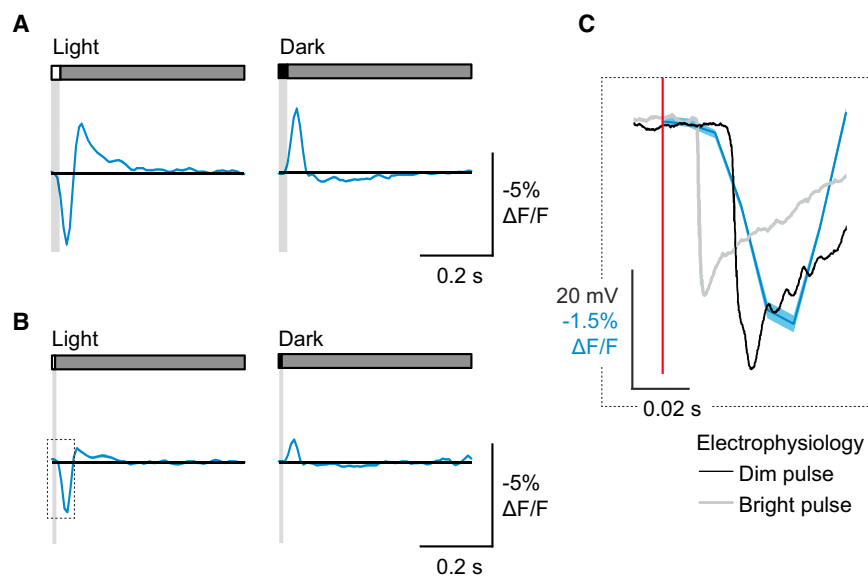


Figure 2. Voltage Imaging Captures L2 Impulse Responses

(A) Response of L2 axon terminals to a 25 ms light flash (left) or a 25 ms dark flash (right), with a 500 ms gray interleave. Contrast = 0.5. $n = 125$ cells, 11 flies.

(B) Response of L2 axon terminals to an 8 ms light flash (left) or an 8 ms dark flash (right), with a 500 ms gray interleave. Contrast = 0.5. $n = 66$ cells, 6 flies.

(C) Response trace in (B) rescaled and plotted with an electrophysiological recording from a lamina monopolar cell responding to similarly brief light flashes of two different intensities (data from Nikolaev et al., 2009). All responses are aligned to the onset of the light flash (red line).

alent to the linear filter that can be extracted using white noise analysis (Chichilnisky, 2001). We therefore presented both 8 ms and 25 ms light and dark flashes off of a uniform gray background to flies in which ASAP2f was expressed

in L2. Such short flashes approximately matched the flicker fusion rate of *Drosophila* photoreceptors (Miall, 1978) and therefore should have been seen by the animal as a single impulse signal instead of a distinct light to dark and dark to light transition for each flash. For both 25 ms and 8 ms flashes, L2 initially hyperpolarized to the light flash and depolarized to the dark flash (Figures 2A and 2B). The response to the light flash was strongly biphasic, with a slower depolarizing phase that followed the initial hyperpolarization. Conversely, the response to the dark flash was only weakly biphasic. Thus, impulse responses to light and dark were not sign-inverted or rescaled versions of the same waveform, suggesting that even at this early stage of visual processing, nonlinearities in voltage responses are significant.

As a critical control, we examined whether the kinetics of these impulse responses were consistent with previous electrophysiological studies. The onset of the impulse response was delayed relative to the onset of light by ~ 17 ms (Figure 2C). This delay was intermediate between the response latencies measured under bright and dim illumination conditions using electrophysiological recordings from lamina monopolar cells (Figure 2C) (Nikolaev et al., 2009). Thus, ASAP2f can report rapid changes in neural activity.

To robustly stimulate L2, we first presented alternating 300 ms full contrast dark and light flashes covering the entire screen. ASAP1 and ASAP2f both reported that L2 transiently depolarized to light offset and transiently hyperpolarized to light onset, consistent with previous electrophysiological recordings (Figures 1F and 1G) (Zettler and Järviö, 1971). The signal amplitudes and signal-to-noise ratios of these indicators were sufficient to record robust single-cell responses; we could also measure responses from single stimulus presentations (Figures 1F and 1G, bottom). ASAP2f produced larger fluorescence changes than ASAP1 ($14.0\% \pm 0.7\%$ increase for depolarization and $20.3\% \pm 1.4\%$ increase for hyperpolarization), with similar response kinetics (Figures 1H–1J). ASAP2f responses were stable for at least 10 min of continuous imaging, facilitating many stimulus presentations (Figures S2D and S2E). We therefore used ASAP2f in subsequent experiments.

ASAP2f Allows Impulse Response Measurements

One commonly used approach to characterizing a dynamic system is to measure the impulse response, the response evoked by an extremely brief stimulus. In visual neuroscience, impulses correspond to brief flashes of light and reveal critical aspects of a cellular response, including the kinetics and waveform (Smith, 1997). For linear systems, the impulse response is equiv-

alent to the linear filter that can be extracted using white noise analysis (Chichilnisky, 2001). We therefore presented both 8 ms and 25 ms light and dark flashes off of a uniform gray background to flies in which ASAP2f was expressed

in L2. Such short flashes approximately matched the flicker fusion rate of *Drosophila* photoreceptors (Miall, 1978) and therefore should have been seen by the animal as a single impulse signal instead of a distinct light to dark and dark to light transition for each flash. For both 25 ms and 8 ms flashes, L2 initially hyperpolarized to the light flash and depolarized to the dark flash (Figures 2A and 2B). The response to the light flash was strongly biphasic, with a slower depolarizing phase that followed the initial hyperpolarization. Conversely, the response to the dark flash was only weakly biphasic. Thus, impulse responses to light and dark were not sign-inverted or rescaled versions of the same waveform, suggesting that even at this early stage of visual processing, nonlinearities in voltage responses are significant.

ASAP2f Reports Voltage Signals across Different Cellular Compartments

Unlike electrophysiological approaches, monitoring neural activity using voltage imaging allows responses to be easily measured from multiple regions of the same neuron. We therefore expressed ASAP2f in the Mi1 cell type, a small monopolar neuron that is representative of interneurons in the fruit fly brain. Mi1 is ~ 50 μm long, with its main neurite being 200–300 nm in diameter and its arbors being comprised of many processes of 200 nm or less (Figure 3A) (Takemura et al., 2013). We measured robust voltage responses in the cell body and the three dendritic and axonal arbors in medulla layers M1, M5, and M10 (Figure 3B).

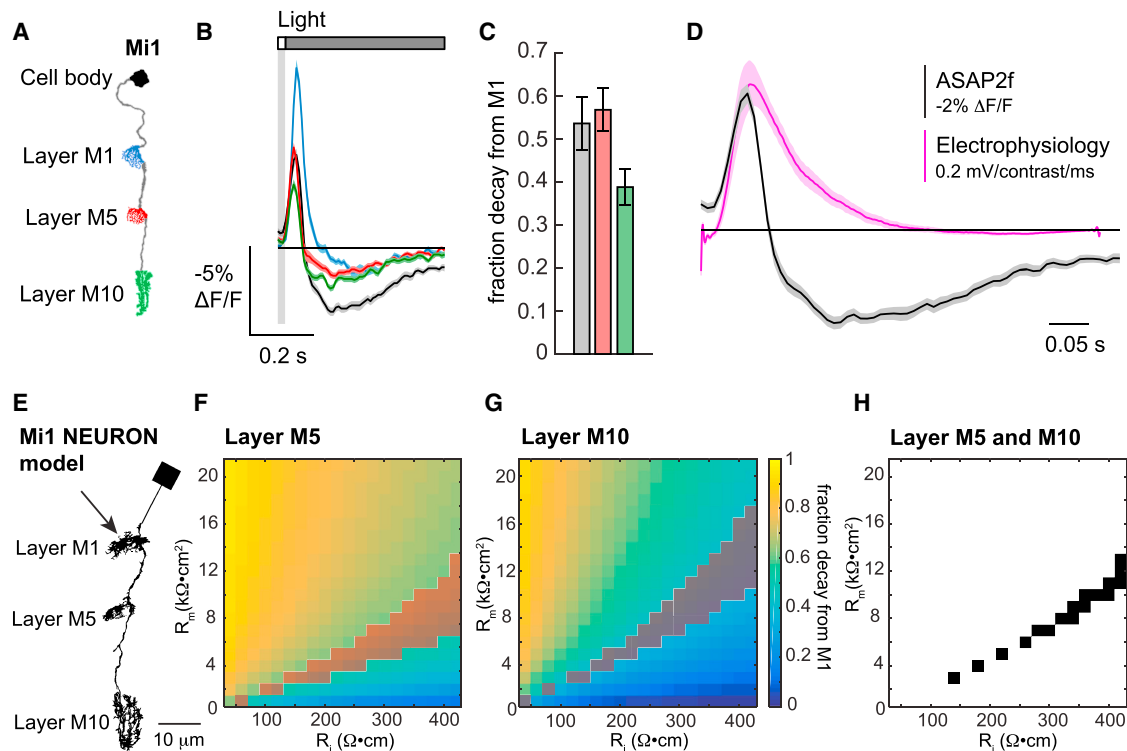


Figure 3. Voltage Imaging Captures Mi1 Response Kinetics and the Decay in Response Amplitude along the Length of the Cell

(A) Illustration of Mi1 with the imaged regions highlighted.

(B) Voltage responses of the Mi1 arbors in layer M1 (blue, $n = 79$ cells, 4 flies), layer M5 (red, $n = 92$ cells, 4 flies), layer M10 (green, $n = 67$ cells, 4 flies), and the cell body (black, $n = 37$ cells, 2 flies) to a 25 ms light flash with a 500 ms gray interleave, contrast = 0.5.

(C) Quantification of the decay in peak response amplitude (peak $\Delta F/F$) as a fraction of the response in layer M1.

(D) Impulse responses measured from the cell body of Mi1. Black: voltage response to a 25 ms light flash measured with ASAP2f (data from B). Pink: linear filter extracted from white noise analysis measured using electrophysiological recordings (data from Behnia et al., 2014).

(E) Morphology of a NEURON model of Mi1. The arrow indicates the site of current injection. The model neuron was given passive membrane properties: specific membrane capacitance (C_m) = 1 $\mu\text{F}/\text{cm}^2$, axial resistance (R_i) = 40 to 420 $\Omega \times \text{cm}$, and specific membrane resistance (R_m) = 1 to 21 $\text{k}\Omega \times \text{cm}^2$.

(F and G) Peak membrane potential during current injection presented as the fraction decayed from the peak response in layer M1. (F) Layer M5 and (G) layer M10 of the NEURON model. The shaded areas indicate the set of R_i and R_m values that result in decay values within 1 SEM of the decay measured with ASAP2f.

(H) The set of R_i and R_m values that result in decay values within 1 SEM of the decay measured with ASAP2f for both layers M5 and M10.

The amplitude of the responses generally decayed away from the site of primary synaptic input in layer M1, but the time courses of the response waveforms were largely preserved throughout the length of the neuron (Figures 3B and 3C). Moreover, our impulse response, the ASAP2f-measured voltage change to a 25 ms light flash and the linear filter extracted from white noise analysis using electrophysiological approaches, both measured in the cell body of Mi1, had indistinguishable times to initial response and times to peak (Figure 3D) (Behnia et al., 2014). However, we note that the impulse response we measured was more biphasic than the linear filter, likely because fast white noise stimuli do not drive temporal and spatial surrounds as well as isolated flashes (Simoncelli et al., 2004).

We next asked whether the decay in the amplitude of the responses along the length of Mi1 was to be expected from the electrical properties of the cell or whether ASAP2f was behaving differently in distinct arbors. Electrode recordings are impossible from these small processes, so we instead implemented a biophysical model of the cell using NEURON (Carnevale and Hines,

2006). We used the morphology from the electron microscopic reconstruction of Mi1 to describe the structure of the arbors in the medulla (Takemura et al., 2013), and as this reconstruction lacked a cell body, we added a simple connecting process and cell body to the model (Figure 3E). We gave the model cell only passive membrane properties and simulated synaptic input by injecting current into the arbor in layer M1, where the neuron receives most of its synapses. From this, we asked whether the decay in amplitude from layer M1 to layers M5 and M10 was consistent with a biologically plausible set of passive membrane properties. Critically, the same parameters should be able to explain the decay amplitude in both layers M5 and M10. To do this, we incorporated previous estimates of the specific membrane capacitance and resting membrane potential and then swept the axial resistance and specific membrane resistance across biologically plausible values (Behnia et al., 2014; Cuntz et al., 2013; Gouwens and Wilson, 2009; Borst and Haag, 1996). These simulations revealed a range of parameter values that predicted the amplitude decay we measured with ASAP2f

in both M5 and M10 (Figures 3F–3H). Thus, ASAP2f appears to accurately report changes in membrane voltage in different neuronal compartments. These simulations also suggest that membrane potential changes spread passively through Mi1, although we do not exclude a role for active conductances.

Voltage Responses Are Transformed in Amplitude, Sign, and Kinetics across Synapses

We next sought to monitor how changes in light intensity are progressively transformed across synapses. We therefore imaged presynaptic axon terminals and their corresponding postsynaptic dendrites while presenting 25 ms light and dark flashes. We first examined responses in the OFF pathway, comparing Tm1 and Tm2 voltage dynamics to those of L2, their presynaptic partner (Figure 4A). Like the axon terminals of L2, the dendrites of Tm1 and Tm2 hyperpolarized to light flashes and depolarized to dark flashes (Figures 4B, S3A, and S3B), consistent with previous electrophysiological recordings from the cell body (Behnia et al., 2014). Additionally, we found that the amplitude of the voltage responses was significantly larger in the postsynaptic dendrite than in the presynaptic axon terminal (Figures 4B, 4C, S3B, and S3C). As these are thought to be non-spiking neurons, this increase in amplitude may boost the voltage signal to ensure reliable propagation to the neurons' distal arbors. Furthermore, the kinetics of the voltage signal were significantly slower in the postsynaptic dendrites: Tm1 and Tm2 responses peaked later and persisted longer than L2 responses (Figures 4B, 4D, 4E, S3B, S3D, and S3E). Mathematically, these responses suggest that Tm1 and Tm2 integrate the L2 voltage signal. As the responses to a 25 ms flash approximate the cells' impulse responses, the slower kinetics of Tm1 and Tm2 demonstrate that at the synapse between L2 and its postsynaptic partners, the circuit becomes tuned for slower changes in light intensity. Finally, we note that Tm2 responses peaked slightly earlier than Tm1 responses, consistent with previous measurements (Behnia et al., 2014).

We next asked whether visual information is transformed differently across synapses in the ON pathway compared to the OFF pathway. In the ON pathway, L1 makes synaptic connections with Mi1 and Tm3 via two axon terminals located in medulla layers M1 and M5 (Takemura et al., 2013). In layer M1, L1 responded very similarly to L2, hyperpolarizing to light increments and depolarizing to light decrements (Figures 4F, 4G, S3F, and S3G). However, unlike the OFF pathway, we observed a sign inversion between L1 and its postsynaptic cells (Figures 4G, 4H, S3G, and S3H), as has been previously reported (Behnia et al., 2014). Interestingly, similar to the transformation between L2 and its postsynaptic targets, Mi1 and Tm3 responses were larger in amplitude and slower in kinetics than those of their presynaptic partner L1 (Figures 4G–4J and S3G–S3J). In layer M5, we observed similar changes in response sign, amplitude, and kinetics to those we saw in layer M1 (Figures 4K–4O and S3K–S3O). Thus, the L1 and L2 pathways perform similar transformations in signal amplitude and kinetics even as they employ synapses of opposite sign, consistent with the view that they are parallel ON and OFF channels. Taken together, these results demonstrate that voltage signals undergo profound transformations in amplitude, sign, and kinetics as they are passed across synapses.

Calcium Responses, Unlike Voltage Responses, Are Compartmentalized within a Neuron

Chemical synaptic transmission requires changes in membrane potential to be converted into changes in intracellular calcium concentration, which then trigger neurotransmitter release (Fatt and Katz, 1952). We therefore compared voltage and calcium signals in corresponding regions of the same neuron. Specifically, we measured voltage signals with ASAP2f and calcium signals with GCaMP6f, a fast variant of the GCaMP family (Chen et al., 2013), across multiple compartments of Tm3, Mi1, and Tm1. In all three cell types, the temporal waveforms of the voltage responses were similar throughout the length of each neuron while the amplitude of the responses decayed away from the site of primary synaptic input (layer M1 for Tm3 and Mi1 and layer M2 for Tm1; Figures 5A, 5B, 5D, 5F, 5G, 5I, S4A, S4B, and S4D), a result consistent with passive spread of membrane potential changes in Tm3, Mi1, and Tm1.

To our surprise, however, unlike voltage signals, calcium signals were highly compartmentalized. That is, calcium responses were different among distinct regions of the same cell and the way in which they were compartmentalized differed among cell types. The calcium signal in any compartment could not be predicted from either the voltage response in that compartment or the calcium responses in other regions of the same cell. For example, in response to a 25 ms light flash, as expected for a depolarization, the calcium concentration increased across all of Tm3 (Figures 5C and 5E). However, inconsistent with the relative amplitudes of the voltage signals in each region, calcium responses in the cell body and layer M5 were much smaller than those in layers M1 and M10, the neighboring regions (Figures 5A–5E). Despite the large differences in the magnitude of intracellular calcium responses, the waveform and kinetics were the same across layers M1, M5, and M10 (Figures 5C and 5E). However, the calcium signals were slower in the cell body. In Mi1, in contrast to Tm3, the relative amplitude of the calcium changes in the different layers of the medulla was consistent with the voltage responses (Figures 5F–5J). However, in this cell, the calcium response waveform in layer M10 was biphasic and relatively fast, while the responses in layers M1 and M5 were monophasic and slower to peak (Figures 5H and 5J). Thus, because Mi1 has synaptic outputs from each of these arbors (Takemura et al., 2013), it could transmit qualitatively different visual information from layer M10 than from layers M1 and M5. Additionally, like Tm3, the calcium responses were the slowest in the Mi1 cell body (Figures 5H and 5J). Finally, in Tm1, unlike Tm3 or Mi1, calcium responses in all arbors were similar in amplitude and kinetics, much like the voltage responses, although the cell body responses were slow and small (Figure S4). Taken together, these results demonstrate that both the amplitude and kinetics of changes in intracellular calcium concentration have distinct relationships with voltage in different compartments of the same cell and are cell type specifically regulated.

ON and OFF Selectivity Arises in the Transformation between Voltage and Calcium

Postsynaptic to Mi1 and Tm3, T4 is strongly selective for light stimuli and hence rectified for ON; postsynaptic to Tm1 and

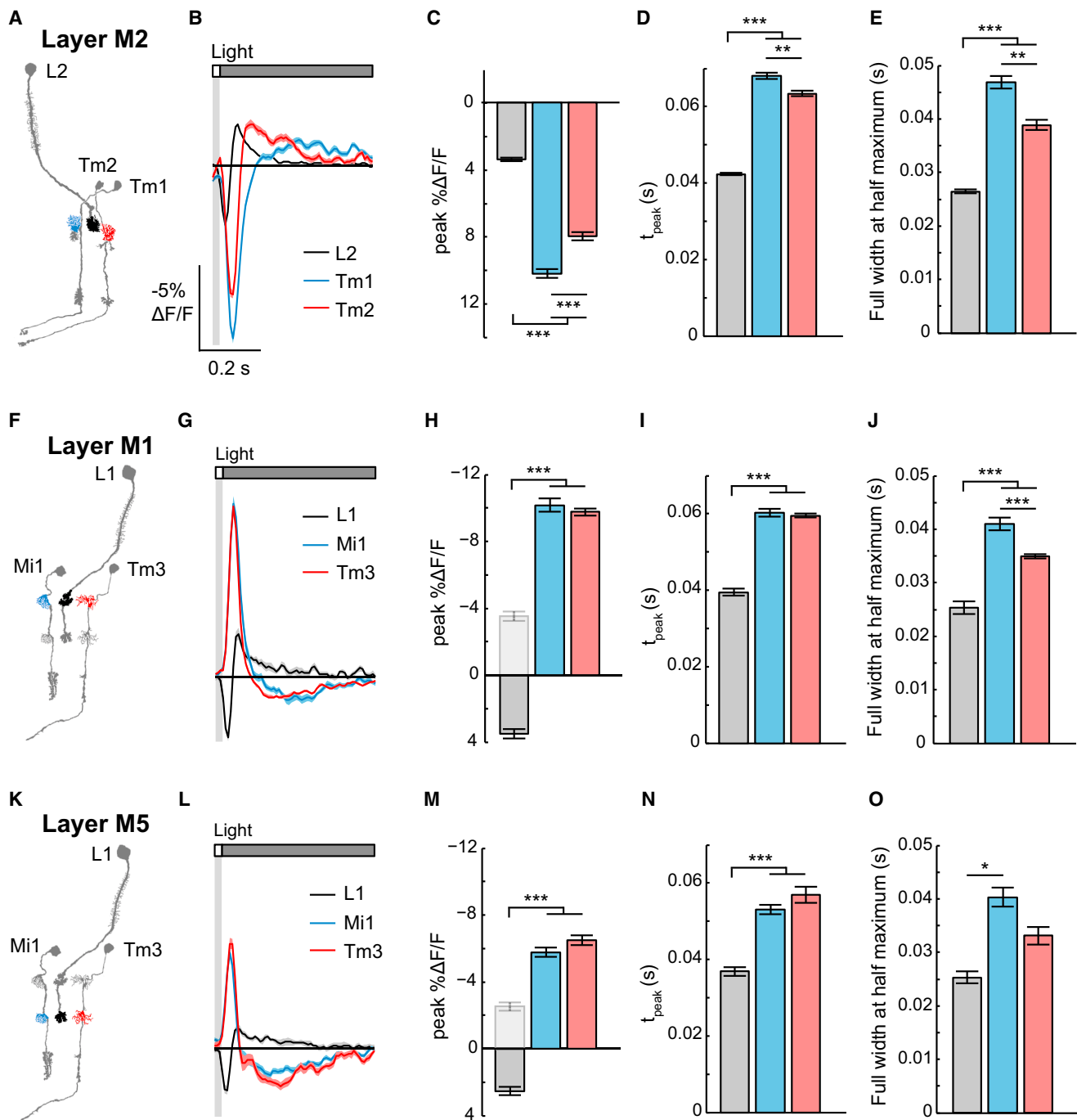


Figure 4. Voltage Responses Are Transformed between Presynaptic Axons and Postsynaptic Dendrites

(A) Illustration of L2 and its postsynaptic targets Tm1 and Tm2. The imaged arbors in medulla layer M2 are highlighted.

(B) Responses of L2 (black, $n = 125$ cells, 11 flies), Tm1 (blue, $n = 79$ cells, 4 flies), and Tm2 (red, $n = 89$ cells, 4 flies) to a 25 ms light flash with a 500 ms gray interleave, contrast = 0.5. The solid line is the mean response; the shading is ± 1 SEM.

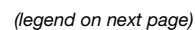
(C–E) Quantification of the response: (C) peak $\Delta F/F$; (D) t_{peak} ; (E) full width at half maximum of the initial response. The mean ± 1 SEM is plotted.

(F–J) In medulla layer M1, presynaptic cell L1 (black, $n = 23$ cells, 6 flies) and postsynaptic cells Mi1 (blue, $n = 79$ cells, 4 flies) and Tm3 (red, $n = 153$ cells, 8 flies).

(K–O) In medulla layer M5, L1 (black, $n = 14$ cells, 5 flies), Mi1 (blue, $n = 92$ cells, 4 flies), and Tm3 (red, $n = 35$ cells, 4 flies).

In (H) and (M), the light gray bar is the inverted L1 peak $\Delta F/F$ for comparison. * $p < 0.05$, ** $p < 0.01$, *** $p < 0.001$ (two-sample t test for peak $\Delta F/F$ and full width at half maximum, Mann-Whitney U test for t_{peak} , Bonferroni correction for multiple comparisons).

See also Figure S3.



Tm2, T5 is strongly selective for dark and hence rectified for OFF (Fisher et al., 2015; Leonhardt et al., 2016; Maisak et al., 2013). However, electrophysiological studies demonstrated that Mi1, Tm3, Tm1, and Tm2 are moderately selective (Behnia et al., 2014), a degree of rectification that cannot account for the nonlinearity of the postsynaptic responses. To map the emergence of rectification across visual circuitry, we presented contrast-matched light and dark flashes spanning six different contrast values to L1 and Tm3, members of the ON pathway, as well as L2 and Tm1, members of the OFF pathway, and measured voltage and calcium responses in their axon terminals.

Voltage signals in L1 and L2 responded strongly to both light and dark, with slightly larger responses to increments of light relative to decrements of equivalent magnitude. Intracellular calcium signals in both cell types responded robustly to both light and dark, but slightly favored decrements, consistent with previous reports (Clark et al., 2011; Juusola et al., 1995) (Figures 6A, 6B, 6D, 6E, 7A, and 7C). Voltage signals in Tm3, like in L1, responded strongly to both light and dark, with a modestly larger response to increments (Figures 6C and 7B). Strikingly, this cell's calcium signals displayed strong, half-wave rectification, with depolarizing changes in membrane potential producing large increases in calcium concentration but hyperpolarizations producing minimal decreases in calcium concentration (Figure 6C). Calcium signals in Tm3 were therefore selective for light: large calcium increases were evoked by light flashes but much smaller calcium decreases were evoked by dark flashes (Figures 6C and 7B). We obtained similar results from the other ON pathway cell, Mi1 (Figures S5A–S5C). Voltage signals in the OFF pathway neuron Tm1 also responded strongly to both light and dark (Figures 6F and 7D). Remarkably, in this cell, calcium signals evoked by decrements were much stronger than those evoked by increments (Figures 6F and 7D). Again, we observed similar results from the other OFF pathway neuron Tm2 (Figures S5D–S5F). Taken together, these data demonstrate that contrast selectivity emerges at the level of the voltage to calcium transformation in the third order neurons of both the ON and OFF pathways.

We were concerned that indicator nonlinearities and not underlying biological processes might account for the rectification we observed. To examine this, we measured contrast responses across these cell types using different voltage and calcium indicators. For voltage, we developed a new member of the ASAP family, ASAP1 I67T Q397R, that had larger fluorescence changes to depolarizations and smaller fluorescence changes

to hyperpolarizations compared with ASAP2f (Figure S6). Using this indicator, we found that the degree of rectification in L2, Tm1, and Tm3 was consistent with that measured with ASAP2f (Figures S7A–S7F). For calcium, we used GCaMP6m, which has a K_d that is approximately half that of GCaMP6f (Chen et al., 2013). If the observed half-wave rectification reflected the fact that GCaMP6f is less sensitive to low calcium concentrations, then the responses measured with GCaMP6m should not be rectified. However, this was not the case, as the degree of rectification was similar for GCaMP6f and GCaMP6m (Figures S7A–S7F). As an independent approach to exploring the effect of indicator nonlinearities on rectification, we also examined whether measurement of GCaMP6f responses to visually evoked hyperpolarization was limited by the ability of the indicator to report calcium decreases. Replacing the perfusion saline with one that contained a calcium chelator, we observed that GCaMP6f fluorescence in L2, Tm1, and Tm3 decreased dramatically, much more than observed when presenting visual stimuli (Figures S7G–S7I). Thus, our measurements are well within GCaMP6f's dynamic range in these cells, a conclusion that is also consistent with our ability to measure the robust calcium increases and decreases evoked by dark and light flashes using this indicator in L1 and L2.

Taken together, these data demonstrate that the degree of linearity of the voltage to calcium transform differs across neurons to implement contrast selectivity (Figure 7E). In L1 and L2, the amplitude of calcium and voltage responses vary largely linearly with respect to contrast. However, in two postsynaptic targets of each cell, calcium responses, but not voltage responses, were strongly half-wave rectified to favor the depolarizing visual stimulus. The upstream synaptic sign inversion between L1 and its postsynaptic partners combined with rectification at the level of intracellular calcium in Mi1 and Tm3 makes the L1 pathway ON selective. The sign preserving synapse between L2 and its postsynaptic partners combined with rectification at the level of calcium in Tm1 and Tm2 makes the L2 pathway OFF selective.

DISCUSSION

The transformation of information by individual neurons and circuits underlies nervous system function. By performing both voltage and calcium imaging of visually evoked responses not only in cell bodies but also in dendrites and axons, we take a novel approach toward understanding information processing. While neurons transmit voltage signals across their processes

Figure 5. Mapping Voltage and Calcium Responses in Different Subcellular Compartments of the Same Neuron

(A) Illustration of Tm3 with the imaged regions highlighted.

(B) Voltage responses of Tm3 arbors in layer M1 (blue, $n = 158$ cells, 8 flies), layer M5 (red, $n = 35$ cells, 4 flies), layer M10 (green, $n = 100$ cells, 9 flies), and the cell body (black, $n = 13$ cells, 2 flies) to a 25 ms light flash with a 500 ms gray interleave, contrast = 0.5.

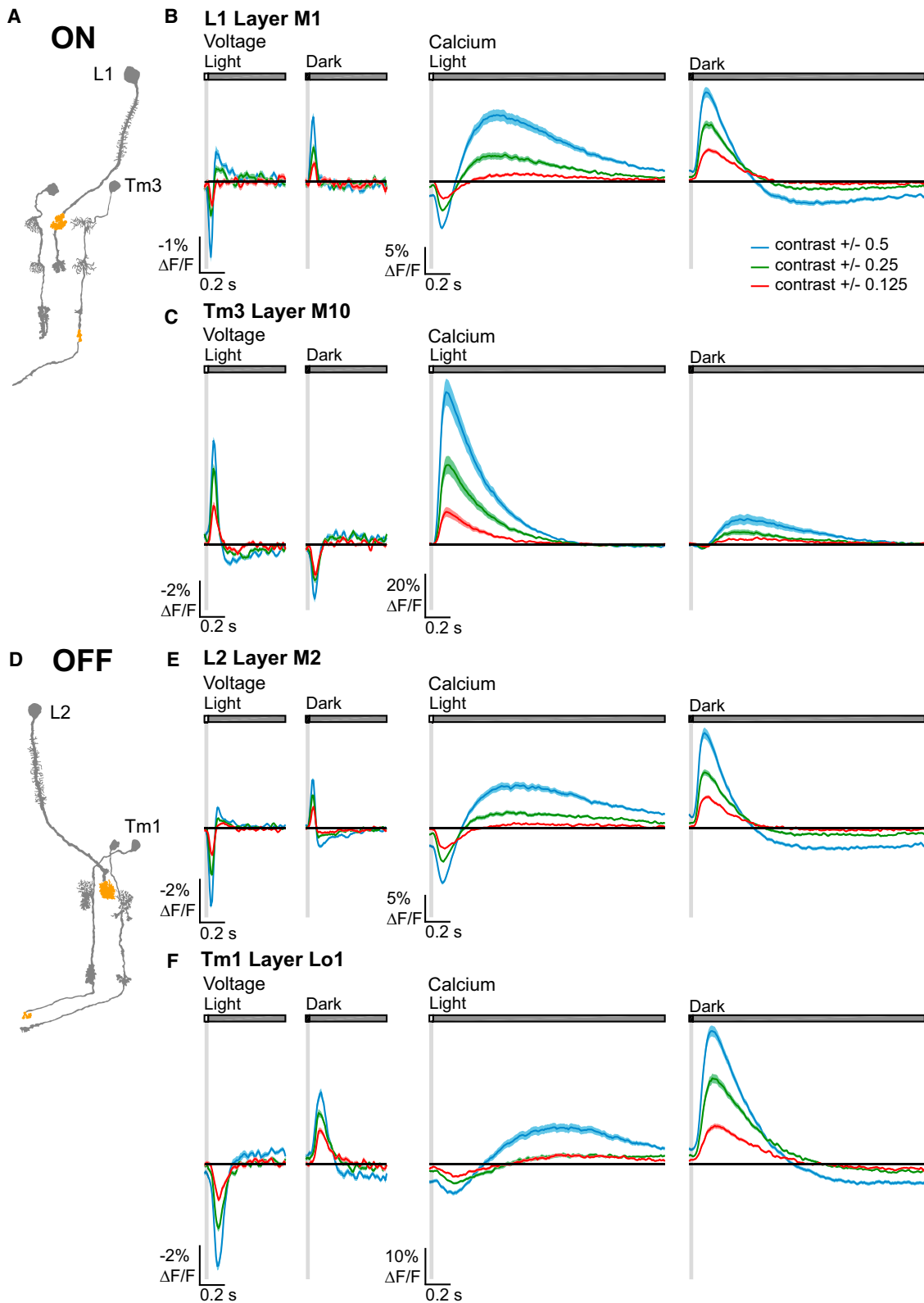
(C) Calcium responses of Tm3 arbors in layer M1 (blue, $n = 126$ cells, 8 flies), layer M5 (red, $n = 69$ cells, 8 flies), layer M10 (green, $n = 99$ cells, 4 flies), and the cell body (black, $n = 71$ cells, 4 flies) to a 25 ms light flash with a 1500 ms gray interleave, contrast = 0.5. The solid line is the mean response; the shading is ± 1 SEM.

(D) Quantification of the voltage signals. Left: peak $\Delta F/F$. Middle: t_{peak} . Right: full width at half maximum. The mean ± 1 SEM is plotted.

(E) Quantification of the calcium signals with the metrics arranged as in (D).

(F–J) Responses of Mi1. (G and I) Voltage responses of the Mi1 arbors in layer M1 (blue, $n = 79$ cells, 4 flies), layer M5 (red, $n = 92$ cells, 4 flies), layer M10 (green, $n = 67$ cells, 4 flies), and the cell body (black, $n = 37$ cells, 2 flies). (G) is repeated from Figure 3B. (H and J) Calcium responses of the Mi1 arbors in layer M1 (blue, $n = 94$ cells, 5 flies), layer M5 (red, $n = 67$ cells, 5 flies), layer M10 (green, $n = 89$ cells, 5 flies), and the cell body (black, $n = 51$ cells, 5 flies). ** $p < 0.01$, *** $p < 0.001$ (two-sample t test for peak $\Delta F/F$ and full width at half maximum, Mann-Whitney U test for t_{peak} , Bonferroni correction for multiple comparisons).

See also Figure S4.



(legend on next page)

with high fidelity, we observe large transformations in the sign, kinetics, and amplitude of visually driven changes in voltage across synapses. Thus, critical neuronal computations are performed between synaptically connected neurites. We also find that calcium responses, unlike voltage responses, are compartmentalized within a neuron. This functional specialization allows an individual neuron to transmit distinct information across different synapses, thereby creating a neural substrate for local computation. Finally, we demonstrate that ON and OFF selectivity, a critical split in sensory processing pathways in many systems, emerges at the voltage to calcium transformation in third-order neurons in this circuit.

Validation of In Vivo Voltage Imaging with Genetically Encoded Indicators

There has been considerable interest in applying genetically encoded voltage indicators to in vivo studies of neuronal computation. These tools hold the promise of allowing measurements of membrane potential changes in subcellular compartments; compared to genetically encoded calcium indicators, they have faster temporal resolution and are a direct readout of voltage changes. However, limitations in the dynamic range, brightness, and critically, the ability to be excited by two-photon stimulation have restricted their use in vivo. Using an improved voltage indicator, we demonstrate that in vivo voltage imaging can provide novel biological insights that could not have been obtained through other techniques.

To validate this new indicator, ASAP2f, we compared ASAP2f responses to previous electrophysiological recordings from the same cells (Figures 1, 2, and 3) (Behnia et al., 2014; Nikolaev et al., 2009). The temporal features revealed by the indicator matched the electrophysiological response profiles well, thereby providing confidence that voltage imaging is an accurate readout of the underlying biological responses. However, a key advantage of imaging is that signals from subcellular regions inaccessible to electrodes can also be measured. To validate these measurements, we took an in silico approach, implementing a simple biophysical model of the cell. These studies revealed that the changes in membrane potential revealed by the indicator are consistent with those predicted by the model cell across physiologically reasonable membrane properties (Figure 3). Thus, ASAP2f appears to accurately report voltage changes across dendrites and axons.

ASAP2f complements other genetically encoded voltage indicators that have been used for in vivo imaging in *Drosophila*, ArcLight and Ace2N-mNeon (Cao et al., 2013; Gong et al., 2015). Using ArcLight, Cao et al. (2013) were the first to measure sensory stimulus-evoked voltage signals in living flies. More

recently, Gong et al. (2015) used Ace2N-mNeon to record similar voltage responses with greatly improved temporal resolution. Both of these studies used epifluorescence illumination; in vivo, two-photon imaging has not been reported for either indicator. ASAP2f performs well under two-photon excitation, and this afforded us two critical advantages. First, we could image in the visual system where one-photon illumination would stimulate the photoreceptors (Salcedo et al., 1999). Second, more generally, the minimal out-of-plane fluorescence of this imaging modality increases the effective spatial resolution in deep tissue, an advantage for mapping neuronal responses with subcellular resolution (Svoboda and Yasuda, 2006). However, we note that while Ace2N-mNeon signals were captured at 1 kHz (Gong et al., 2015), our signals were sampled at 120 Hz, a difference that reflects the distinct imaging modalities used. Nonetheless, two-photon imaging of ASAP2f will be broadly applicable to experimental systems where the advantages of two-photon excitation are required.

More generally, from the perspective of reporters of neuronal activity, we provide definitive evidence that voltage and calcium changes are distinct signals (Figures 5, 6, and 7). This demonstrates the need for careful interpretation of responses measured with different indicators but also the need for sensors of different aspects of neuronal activity to provide a richer picture of nervous system function.

Neuronal Computations Occur between Synaptically Connected Neurites

Taking advantage of cell-type-specific indicator expression and sufficient spatial resolution and indicator sensitivity to measure signals from subcellular compartments, we observed information flow between synaptically connected axons and dendrites. Across four different synapses, we found transformations in the amplitude and kinetics of voltage signals evoked by sensory stimuli in vivo (Figure 4). Voltage responses to identical visual stimuli were larger in the postsynaptic dendrite than they were in the axon. This amplification may enable reliable passive propagation of weak input signals to the axon terminal of the postsynaptic cell. Given the relatively poor quantum efficiency of the fly compound eye, this amplification may be critical to the transmission of low contrast visual inputs. In addition, across all four synaptic connections, initial postsynaptic voltage signals emerged with a short latency relative to the presynaptic signal but evolved more slowly and appeared to integrate it. As these cells represent critical inputs to neurons that compute the direction of motion (Shinomiya et al., 2014; Takemura et al., 2013), these temporal transformations tune the speed sensitivity of motion detectors. More broadly, our results emphasize the central role

Figure 6. Measuring ON and OFF Selectivity

(A) Illustration of the ON pathway with the imaged regions highlighted.

(B and C) Voltage (left) and calcium (right) responses of (B) L1 (voltage: $n = 43$ cells, 9 flies and calcium: $n = 68$ cells, 9 flies) and (C) Tm3 (voltage: $n = 97$ cells, 8 flies and calcium: $n = 85$ cells, 7 flies) to 25 ms light and dark flashes of varying contrasts off of gray (contrast = 0.125, 0.25, or 0.5). The solid line is the mean response; the shading is ± 1 SEM.

(D) Illustration of the OFF pathway.

(E and F) Voltage (left) and calcium (right) responses of (E) L2 (voltage: $n = 116$ cells, 7 flies and calcium: $n = 88$ cells, 8 flies) and (F) Tm1 (voltage: $n = 84$ cells, 7 flies and calcium: $n = 136$ cells, 8 flies).

See also Figures S5, S6, and S7.

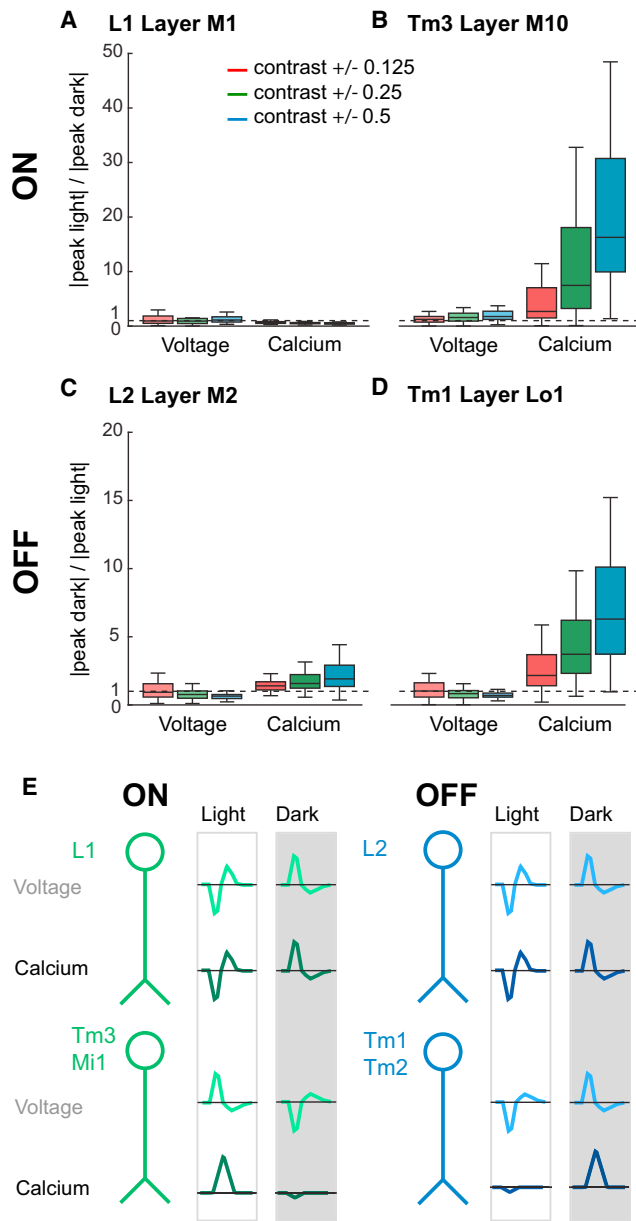


Figure 7. ON and OFF Selectivity Arises in the Transformation between Voltage and Calcium

(A and B) Quantification of selectivity to light (ON). The line, box, and whiskers are the median, interquartile range, and maximum and minimum values within one interquartile range, respectively. (A) L1 layer M1 axon terminals (voltage: $n = 43$ cells, 9 flies and calcium: $n = 68$ cells, 9 flies). (B) Tm3 layer M10 axon terminals (voltage: $n = 97$ cells, 8 flies and calcium: $n = 85$ cells, 7 flies). (C and D) Quantification of selectivity to dark (OFF). (C) L2 layer M2 axon terminals (voltage: $n = 116$ cells, 7 flies and calcium: $n = 88$ cells, 8 flies). (D) Tm1 layer Lo1 axon terminals (voltage: $n = 84$ cells, 7 flies and calcium: $n = 136$ cells, 8 flies).

(E) Schematic summarizing the emergence of ON and OFF selectivity, displaying idealized impulse responses, at the level of membrane potential and intracellular calcium.

See also Figures S5, S6, and S7.

that synaptic connections play in precisely shaping processing of behaviorally relevant information in the brain.

Compartmentalization of Calcium Responses Can Support Local Computation

Individual neurons are powerful computational elements, implementing combinations of arithmetic and logical operations to nonlinearly combine inputs to support behaviorally relevant computations in vivo (London and Häusser, 2005; Stuart and Spruston, 2015). However, most studies have focused on how inputs are transformed, making the implicit assumption that a neuron has one output signal that is captured by its pattern of action potential firing. Theoretical studies have instead proposed that further computation can occur after the action potential is generated, perhaps in the transformation between voltage and calcium or between calcium and neurotransmitter release (Abbott and Regehr, 2004). Significantly, this would allow different axon terminals of the same neuron to send different output signals; a neuron would therefore communicate distinct information to its various postsynaptic partners, increasing the opportunity for local circuit computation.

In this study, we found that the medulla neurons Tm3 and Mi1 have the necessary properties to allow this. While they are not spiking neurons, the voltage responses throughout these cells were fundamentally similar in waveform and kinetics (Figure 5). In contrast, the calcium responses differed in amplitude or kinetics among subcellular compartments in a manner that could not be predicted from the voltage responses. As calcium is required for neurotransmitter release and as these regions all contain presynaptic active zones, Tm3 and Mi1 could be conveying multiple distinct streams of information. We speculate that differential regulation of voltage-gated calcium channel density, threshold, or kinetics across the cell could account for the compartmentalization of calcium responses. For example, Ca_v2 - and Ca_v3 -type voltage-gated calcium channels in *Drosophila* antennal lobe projection neurons (PNs) mediate sustained and transient calcium currents, respectively (Gu et al., 2009; Iniguez et al., 2013). Differential distribution of these two types of channels within a neuron could produce compartments with distinct calcium response kinetics.

The Emergence of ON and OFF Selectivity

Vertebrate and invertebrate visual systems have parallel ON and OFF selective pathways that process light and dark, respectively. This fundamental organization parallels the dichotomy between light and dark in natural scenes, and exploitation of this feature of the visual world has been proposed to be computationally advantageous in a variety of ways (Clark et al., 2014; Gjorgjieva et al., 2014; Westheimer, 2007). In this study, we found that the selectivity in neuronal responses for ON and OFF arises specifically at the transformation between voltage and calcium in third-order neurons (Figures 6 and 7). Previous electrophysiological recordings from Tm3, Mi1, Tm1, and Tm2 observed modest half-wave rectification (Behnia et al., 2014). Our voltage imaging experiments revealed a similar degree of rectification in Tm3 and slightly less rectification in the other neurons. Given the demands of two-photon imaging, our stimuli are notably dimmer and have distinct spectral content from those

used previously. Light intensity affects response linearity in the fly visual system (Laughlin et al., 1987); as a result, these minor technical differences are likely to account for the observed differences in rectification between the studies. Nonetheless, the rectification in calcium signals that we observed was stronger than the rectification seen in the voltage measurements and was sufficient to account for the strong selectivity reported in these neurons' postsynaptic partners T4 and T5 (Fisher et al., 2015; Leonhardt et al., 2016; Maisak et al., 2013). The voltage to calcium transformation implements half-wave rectification by producing an increase in calcium concentration upon depolarization but little decrease in calcium concentration upon hyperpolarization. Therefore, to create selectivity for both ON and OFF, there must be an additional sign inversion in one pathway so that both an increase in light and a decrease in light cause depolarization. We observe this sign inversion in the ON pathway (Figure 4). The synaptic sign inversion between L1 and its postsynaptic partners combined with rectification at the level of intracellular calcium signals in Mi1 and Tm3 makes the L1 pathway ON selective. The sign preserving synapse between L2 and its postsynaptic partners combined with rectification at the level of calcium signals in Tm1 and Tm2 makes the L2 pathway OFF selective.

We speculate that thresholding by voltage-gated calcium channels underpins this half-wave rectification. Indeed, distinct low-voltage-activated and high-voltage-activated calcium currents mediated by the Ca_v2 -type voltage-gated calcium channel have been reported in a *Drosophila* motor neuron (Ryglewski et al., 2012). Intriguingly, in the vertebrate retina, voltage responses in many bipolar cells are linear with respect to contrast (Baccus and Meister, 2002; Rieke, 2001), but at the synapse between bipolar cells and retinal ganglion cells, the output is half-wave rectified (Demb et al., 2001; Enroth-Cugell and Freeman, 1987). These results, combined with our data, suggest that rectification through a transformation between voltage and calcium could be a mechanism conserved across phyla for producing the computationally critical response property of ON and OFF selectivity.

Considering our study more broadly, we directly observe the transformations in signal gain, kinetics, and linearity that represent neural computation within cells and across synapses. This approach of in vivo voltage and calcium imaging in subcellular compartments can be applied to other systems. By identifying where and how elementary transformations occur within a circuit, our results pave the way for future studies determining the molecular implementations of neural computation.

EXPERIMENTAL PROCEDURES

In vivo imaging experiments were performed on adult female *Drosophila*. UAS-ASAP2f, UAS-GCaMP6f, UAS-ASAP1 I67T Q397R, and UAS-GCaMP6m were expressed cell-type specifically using the *R48A08AD*; *R66A01DBD* split Gal4 (L1), *21D-Gal4* (L2), *R19F01-Gal4* (Mi1), *R13E12-Gal4* (Tm3), *R74G01-Gal4* (Tm1), and *otd-Gal4*; *GMR-Gal80* (Tm2) driver lines. Unless otherwise specified, all voltage responses were measured with ASAP2f, and all calcium responses were measured with GCaMP6f. Neurons were imaged with two-photon microscopy (excitation wavelength: 920 nm). Emitted photons were collected with a 525/50 nm bandpass filter. Data were acquired at 38.9 Hz and resampled to 120 Hz during post hoc analysis. Visual stimuli were filtered

with a 447/60 nm bandpass filter and projected onto a screen in front of the fly. The screen spanned $\sim 80^\circ$ of the fly's visual field horizontally and 50° vertically. The stimuli presented were: 300 ms alternating full contrast light and dark flashes; 8.33 ms light and dark flashes interleaved with 500 ms of gray, Michaelson contrast = 0.5; and 25 ms light and dark flashes interleaved with 500 ms or 1500 ms of gray, Michaelson contrast = 0.5, 0.25, or 0.125. All stimuli were presented to cover the entire screen. The quantification metrics for the responses to 300 ms flashes were peak $\Delta F/F$, the largest value of the amplitude of the fluorescence change; t_{peak} , the time at which the peak $\Delta F/F$ occurs; and τ_{decay} , the time constant of the decay from the peak $\Delta F/F$. The quantification metrics for the responses to 25 ms flashes were peak $\Delta F/F$; t_{peak} ; and the full width at half maximum of the initial response phase. Selectivity for ON and OFF was computed as: $|\text{peak light response/peak dark response}|$ for the ON pathway and $|\text{peak dark response/peak light response}|$ for the OFF pathway. The peak response was quantified as the maximal $\Delta F/F$ of the initial response phase minus the average $\Delta F/F$ value before the response. See the [Supplemental Experimental Procedures](#) for detailed methods.

SUPPLEMENTAL INFORMATION

Supplemental Information includes Supplemental Experimental Procedures, seven figures and one table and can be found with this article online at <http://dx.doi.org/10.1016/j.cell.2016.05.031>.

AUTHOR CONTRIBUTIONS

H.H.Y. and F.S.-P. designed and performed experiments, analyzed data, and wrote the manuscript. X.S. and X.D. performed experiments. M.Z.L. provided advice and supervision. T.R.C. wrote the manuscript and provided advice and supervision.

ACKNOWLEDGMENTS

We thank L. Luo, S. Baccus, and members of the T.R.C. lab for comments on the manuscript. We thank Y. Geng, M. Hintze, and S. Ganesan for providing dissociated neurons. We thank C. Desplan for the *otd-Gal4* driver line and M. Wernet for building the *GMR-Gal80*; *otd-Gal4* driver line. Cytometry data were collected on an instrument in the Stanford Shared FACS Facility supported by NIH shared instrument grant S10RR027431-01. Two-photon photobleaching data were collected using equipment from the Stanford Neuroscience Microscopy Service, supported by NIH NS069375; training and use of this equipment was supported by a two-photon pilot grant from the Stanford Neurosciences Institute. This work was supported by National Science Foundation grant 1134416 (to F.S.-P. and M.Z.L.), Defense Advanced Research Projects Agency (DARPA) grant W911NF-14-1-0013 (to M.Z.L.), NIH Brain Initiative grant 1U01NS090600-01 (to M.Z.L.), and NIH grants R01 EY022638 (to T.R.C.) and R21 NS081507 (to T.R.C.). H.H.Y. is supported by a Stanford Graduate Fellowship and a Stanford Interdisciplinary Graduate Fellowship. M.Z.L. receives funding from the Rita Allen Foundation and the Burroughs Wellcome Fund. F.S.-P. and M.Z.L. have filed a patent application for a voltage sensor design that includes the sensors reported in this paper.

Received: March 3, 2016

Revised: April 19, 2016

Accepted: May 6, 2016

Published: June 2, 2016

REFERENCES

- Abbott, L.F., and Regehr, W.G. (2004). Synaptic computation. *Nature* 431, 796–803.
- Baccus, S.A., and Meister, M. (2002). Fast and slow contrast adaptation in retinal circuitry. *Neuron* 36, 909–919.
- Behnia, R., Clark, D.A., Carter, A.G., Clandinin, T.R., and Desplan, C. (2014). Processing properties of ON and OFF pathways for *Drosophila* motion detection. *Nature* 512, 427–430.

- Borst, A. (2014). Fly visual course control: behaviour, algorithms and circuits. *Nat. Rev. Neurosci.* 15, 590–599.
- Borst, A., and Haag, J. (1996). The intrinsic electrophysiological characteristics of fly lobula plate tangential cells: I. Passive membrane properties. *J. Comput. Neurosci.* 3, 313–336.
- Cao, G., Platasa, J., Pieribone, V.A., Raccuglia, D., Kunst, M., and Nitabach, M.N. (2013). Genetically targeted optical electrophysiology in intact neural circuits. *Cell* 154, 904–913.
- Camevale, N.T., and Hines, M.L. (2006). *The NEURON Book* (Cambridge University Press).
- Chalasani, S.H., Chronis, N., Tsubozaki, M., Gray, J.M., Ramot, D., Goodman, M.B., and Bargmann, C.I. (2007). Dissecting a circuit for olfactory behaviour in *Caenorhabditis elegans*. *Nature* 450, 63–70.
- Chen, T.-W., Wardill, T.J., Sun, Y., Pulver, S.R., Renninger, S.L., Baohan, A., Schreiter, E.R., Kerr, R.A., Orger, M.B., Jayaraman, V., et al. (2013). Ultrasensitive fluorescent proteins for imaging neuronal activity. *Nature* 499, 295–300.
- Chichilnisky, E.J. (2001). A simple white noise analysis of neuronal light responses. *Network* 12, 199–213.
- Clark, D.A., Bursztyn, L., Horowitz, M.A., Schnitzer, M.J., and Clandinin, T.R. (2011). Defining the computational structure of the motion detector in *Drosophila*. *Neuron* 70, 1165–1177.
- Clark, D.A., Fitzgerald, J.E., Ales, J.M., Gohl, D.M., Silies, M.A., Norcia, A.M., and Clandinin, T.R. (2014). Flies and humans share a motion estimation strategy that exploits natural scene statistics. *Nat. Neurosci.* 17, 296–303.
- Cuntz, H., Forstner, F., Schnell, B., Ammer, G., Raghu, S.V., and Borst, A. (2013). Preserving neural function under extreme scaling. *PLoS ONE* 8, e71540.
- Demb, J.B., Zaghloul, K., Haarsma, L., and Sterling, P. (2001). Bipolar cells contribute to nonlinear spatial summation in the brisk-transient (Y) ganglion cell in mammalian retina. *J. Neurosci.* 21, 7447–7454.
- Enroth-Cugell, C., and Freeman, A.W. (1987). The receptive-field spatial structure of cat retinal Y cells. *J. Physiol.* 384, 49–79.
- Fatt, P., and Katz, B. (1952). Spontaneous subthreshold activity at motor nerve endings. *J. Physiol.* 117, 109–128.
- Fischbach, K.-F., and Dittrich, A.P. (1989). The optic lobe of *Drosophila melanogaster*. I: A Golgi analysis of wild-type structure. *Cell Tissue Res.* 258, 441–475.
- Fisher, Y.E., Silies, M., and Clandinin, T.R. (2015). Orientation Selectivity Sharpens Motion Detection in *Drosophila*. *Neuron* 88, 390–402.
- Gjorgjieva, J., Sompolinsky, H., and Meister, M. (2014). Benefits of pathway splitting in sensory coding. *J. Neurosci.* 34, 12127–12144.
- Gong, Y., Huang, C., Li, J.Z., Grewe, B.F., Zhang, Y., Eismann, S., and Schnitzer, M.J. (2015). High-speed recording of neural spikes in awake mice and flies with a fluorescent voltage sensor. *Science* 350, 1361–1366.
- Gouwens, N.W., and Wilson, R.I. (2009). Signal propagation in *Drosophila* central neurons. *J. Neurosci.* 29, 6239–6249.
- Gu, H., Jiang, S.A., Campusano, J.M., Iniguez, J., Su, H., Hoang, A.A., Lavian, M., Sun, X., and O'Dowd, D.K. (2009). Cav2-type calcium channels encoded by *cac* regulate AP-independent neurotransmitter release at cholinergic synapses in adult *Drosophila* brain. *J. Neurophysiol.* 101, 42–53.
- Iniguez, J., Schutte, S.S., and O'Dowd, D.K. (2013). Cav3-type $\alpha 1T$ calcium channels mediate transient calcium currents that regulate repetitive firing in *Drosophila* antennal lobe PNs. *J. Neurophysiol.* 110, 1490–1496.
- Joesch, M., Schnell, B., Raghu, S.V., Reiff, D.F., and Borst, A. (2010). ON and OFF pathways in *Drosophila* motion vision. *Nature* 468, 300–304.
- Juusola, M., Uusitalo, R.O., and Weckström, M. (1995). Transfer of graded potentials at the photoreceptor-interneuron synapse. *J. Gen. Physiol.* 105, 117–148.
- Kuffler, S.W. (1953). Discharge patterns and functional organization of mammalian retina. *J. Neurophysiol.* 16, 37–68.
- Laughlin, S.B., Howard, J., and Blakeslee, B. (1987). Synaptic limitations to contrast coding in the retina of the blowfly *Calliphora*. *Proc. R. Soc. Lond. B Biol. Sci.* 231, 437–467.
- Leonhardt, A., Ammer, G., Meier, M., Serbe, E., Bahl, A., and Borst, A. (2016). Asymmetry of *Drosophila* ON and OFF motion detectors enhances real-world velocity estimation. *Nat. Neurosci.* 19, 706–715.
- Liu, W.W., Mazor, O., and Wilson, R.I. (2015). Thermosensory processing in the *Drosophila* brain. *Nature* 519, 353–357.
- London, M., and Häusser, M. (2005). Dendritic computation. *Annu. Rev. Neurosci.* 28, 503–532.
- Maisak, M.S., Haag, J., Ammer, G., Serbe, E., Meier, M., Leonhardt, A., Schilling, T., Bahl, A., Rubin, G.M., Nern, A., et al. (2013). A directional tuning map of *Drosophila* elementary motion detectors. *Nature* 500, 212–216.
- Miall, R. (1978). The flicker fusion frequencies of six laboratory insects, and the response of the compound eye to mains fluorescent “ripple”. *Physiol. Entomol.* 3, 99–106.
- Nikolaev, A., Zheng, L., Wardill, T.J., O’Kane, C.J., de Polavieja, G.G., and Juusola, M. (2009). Network adaptation improves temporal representation of naturalistic stimuli in *Drosophila* eye: II mechanisms. *PLoS ONE* 4, e4306.
- Rieke, F. (2001). Temporal contrast adaptation in salamander bipolar cells. *J. Neurosci.* 21, 9445–9454.
- Ryglewski, S., Lance, K., Levine, R.B., and Duch, C. (2012). Ca(v)2 channels mediate low and high voltage-activated calcium currents in *Drosophila* motoneurons. *J. Physiol.* 590, 809–825.
- Salcedo, E., Huber, A., Henrich, S., Chadwell, L.V., Chou, W.H., Paulsen, R., and Britt, S.G. (1999). Blue- and green-absorbing visual pigments of *Drosophila*: ectopic expression and physiological characterization of the R8 photoreceptor cell-specific Rh5 and Rh6 rhodopsins. *J. Neurosci.* 19, 10716–10726.
- Scholl, B., Gao, X., and Wehr, M. (2010). Nonoverlapping sets of synapses drive on responses and off responses in auditory cortex. *Neuron* 65, 412–421.
- Shinomiya, K., Karuppururai, T., Lin, T.-Y., Lu, Z., Lee, C.-H., and Meinertzhagen, I.A. (2014). Candidate neural substrates for off-edge motion detection in *Drosophila*. *Curr. Biol.* 24, 1062–1070.
- Silies, M., Gohl, D.M., and Clandinin, T.R. (2014). Motion-detecting circuits in flies: coming into view. *Annu. Rev. Neurosci.* 37, 307–327.
- Simoncelli, E.P., Paninski, L., Pillow, J., and Schwartz, O. (2004). Characterization of neural responses with stochastic stimuli. In *The Cognitive Neuroscience*, III, M. Gazzaniga, ed. (MIT Press), pp. 327–338.
- Smith, S.W. (1997). *The Scientist and Engineer’s Guide to Digital Signal Processing* (California Technical Publishing).
- St-Pierre, F., Marshall, J.D., Yang, Y., Gong, Y., Schnitzer, M.J., and Lin, M.Z. (2014). High-fidelity optical reporting of neuronal electrical activity with an ultrafast fluorescent voltage sensor. *Nat. Neurosci.* 17, 884–889.
- Stuart, G.J., and Spruston, N. (2015). Dendritic integration: 60 years of progress. *Nat. Neurosci.* 18, 1713–1721.
- Svoboda, K., and Yasuda, R. (2006). Principles of two-photon excitation microscopy and its applications to neuroscience. *Neuron* 50, 823–839.
- Takemura, S.Y., Bharioke, A., Lu, Z., Nern, A., Vitaladevuni, S., Rivlin, P.K., Katz, W.T., Olbris, D.J., Plaza, S.M., Winston, P., et al. (2013). A visual motion detection circuit suggested by *Drosophila* connectomics. *Nature* 500, 175–181.
- Wässle, H. (2004). Parallel processing in the mammalian retina. *Nat. Rev. Neurosci.* 5, 747–757.
- Westheimer, G. (2007). The ON-OFF dichotomy in visual processing: from receptors to perception. *Prog. Retin. Eye Res.* 26, 636–648.
- Zettler, F., and Järvilehto, M. (1971). Decrement-free conduction of graded potentials along the axon of a monopolar neuron. *Z. Vgl. Physiol.* 75, 402–421.

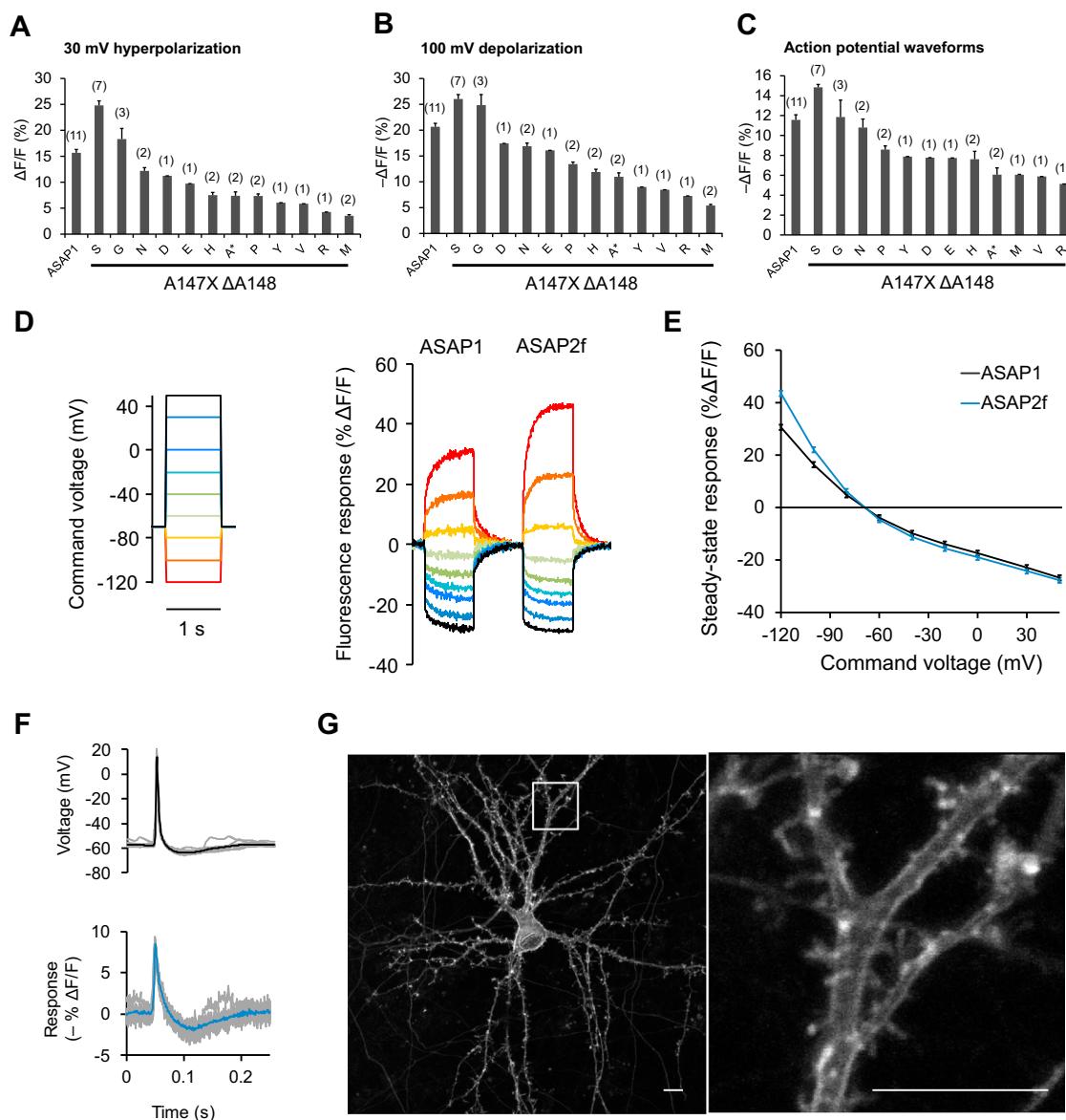


Figure S1. Development of the ASAP2f Voltage Sensor, Related to Figure 1

(A–C) Mean maximal response of ASAP1 variants to (A) a 1 s 30 mV hyperpolarization, (B) a 1 s 100 mV depolarization, or (C) an artificial action potential waveform in HEK293A cells. The label represents the amino acid substituted in the place of A147 in ASAP1 A147X Δ A148 variants. The asterisks denote the original amino acid at position 147 (alanine). Errors bars are \pm 1 SEM. The number of cells tested is shown in parentheses above the bars.

(D) Representative fluorescence responses of ASAP1 and ASAP2f to voltage steps from -120 to 50 mV in HEK293A cells. Responses were measured at 5 ms intervals and were normalized to the fluorescence at the -70-mV holding potential.

(E) Mean fluorescence response to transmembrane voltage of ASAP1 (n = 6) and ASAP2f (n = 6).

(F) Responses of ASAP2f to action potentials in a representative cultured hippocampal neuron. The thick trace is the mean response over all action potentials (n = 17). Single-trial traces are shown in gray.

(G) ASAP2f fluorescence is well-localized at the plasma membrane in a rat cortical neuron, imaged by confocal microscopy. Right: magnified image of the boxed region. Scale bar, 10 μ m.

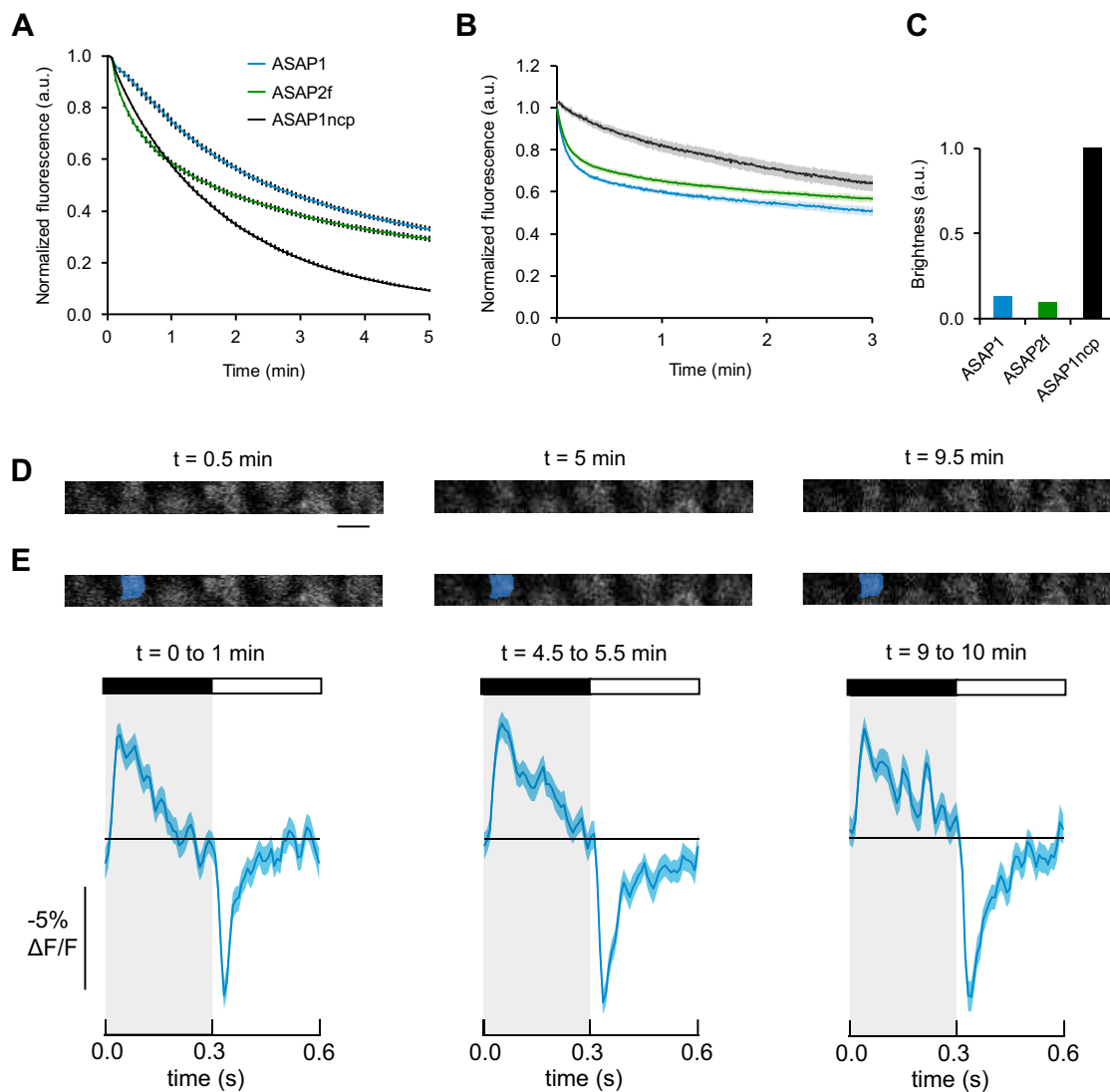


Figure S2. Photostability of ASAP Indicators In Vitro and In Vivo, Related to Figure 1

(A–C) Photostability and brightness of ASAP1, ASAP2f, and ASAP1ncp (a voltage insensitive variant of ASAP1 where cpGFP is replaced with non-circularly permuted EGFP) in HEK293-Kir2.1 cells. (A) One-photon photobleaching kinetics. Cells transiently expressing a voltage sensor were illuminated with 470- to 490-nm light at 10.7 mW/mm² at the sample plane. Fluorescence was normalized to 1.0 at $t = 0$ and averaged over all cells. Error bars are ± 1 SEM (B) Two-photon photobleaching kinetics. Cells transiently expressing each voltage sensor were illuminated with a Ti:sapphire laser tuned to 920 nm and set to a power level of 4.7 mW at the stage. Each pixel was sampled at 2.23 Hz with a dwell time of 0.4 μ s. Fluorescence was normalized to 1.0 at $t = 0$ and averaged over all cells. Shading is ± 1 SEM (C) Fluorescence emission of cells transiently expressing ASAP1, ASAP2f, or ASAP1ncp was measured by flow cytometry. To normalize for sample-to-sample differences in gene expression or transfection efficiency, each sensor variant was genetically fused to the RFP FusionRed. Brightness was quantified as GFP fluorescence divided by RFP fluorescence. Untransfected cells were excluded. $n > 1000$ cells per construct.

(D and E) Continuous in vivo, two-photon imaging of ASAP2f in L2 over 10 min. (D) Example individual imaging frames taken at the indicated times relative to the start of imaging. Scale bar, 5 μ m. (E) Mean response of the highlighted example axon terminal during the indicated 1 min segments to alternating 300 ms-long dark and light flashes. The solid line is the mean response; the shading is ± 1 SEM.

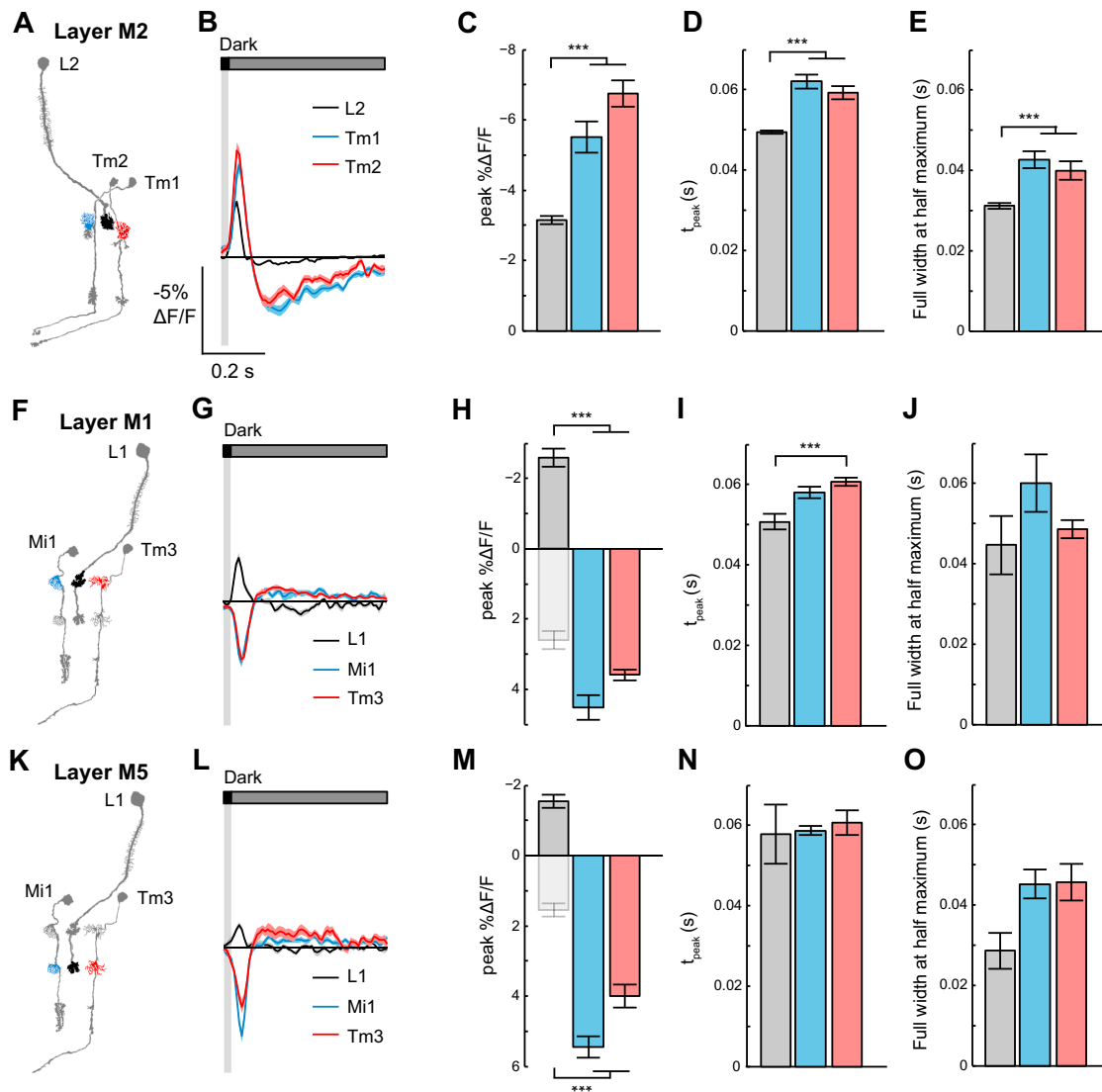


Figure S3. Voltage Responses in Presynaptic Axons and Postsynaptic Dendrites to a 25 ms Dark Flash, Related to Figure 4

(A) Illustration of L2 and postsynaptic cells Tm1 and Tm2. The imaged terminals in medulla layer M2 are highlighted.

(B) Responses of L2 (black, $n = 125$ cells, 11 flies), Tm1 (blue, $n = 79$ cells, 4 flies), and Tm2 (red, $n = 89$ cells, 4 flies) to a 25 ms dark flash with a 500 ms gray interleave, contrast = 0.5. The solid line is the mean response; the shading is ± 1 SEM.

(C–E) Parameters quantifying the response: (C) peak $\Delta F/F$, (D) t_{peak} , (E) full width at half maximum. The mean ± 1 SEM is plotted.

(F–J) In medulla layer M1, L1 (black, $n = 23$ cells, 6 flies), Mi1 (blue, $n = 79$ cells, 4 flies), and Tm3 (red, $n = 153$ cells, 8 flies).

(K–O) In medulla layer M5, L1 (black, $n = 14$ cells, 5 flies), Mi1 (blue, $n = 92$ cells, 4 flies), and Tm3 (red, $n = 35$ cells, 4 flies). In (H) and (M), the light gray bar denotes the inverted L1 peak $\Delta F/F$. *** $p < 0.001$ (two-sample t test for peak $\Delta F/F$ and full width at half maximum, Mann-Whitney U test for t_{peak} , Bonferroni correction for multiple comparisons).

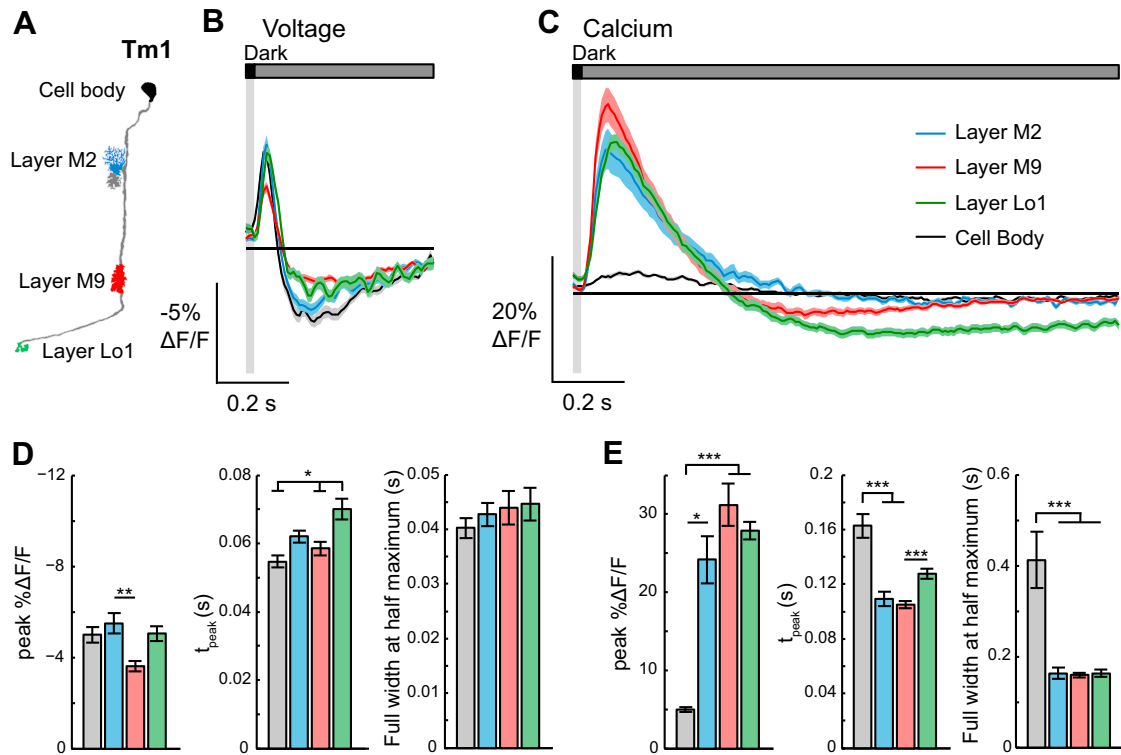


Figure S4. Voltage and Calcium Responses in Different Compartments of Tm1, Related to Figure 5

(A) Illustration of Tm1 with the imaged regions highlighted.

(B) Voltage responses of Tm1 arbors in layer M2 (blue, $n = 79$ cells, 4 flies), layer M9 (red, $n = 99$ cells, 3 flies), layer Lo1 (green, $n = 30$ cells, 3 flies), and the cell body (black, $n = 23$ cells, 2 flies) to a 25 ms dark flash with a 500 ms gray interleave, contrast = 0.5.

(C) Calcium responses of Tm1 arbors in layer M2 (blue, $n = 30$ cells, 8 flies), layer M9 (red, $n = 101$ cells, 10 flies), layer Lo1 (green, $n = 127$ cells, 9 flies), and the cell body (black, $n = 27$ cells, 6 flies) to a 25 ms dark flash with a 1500 ms gray interleave, contrast = 0.5. The solid line is the mean response; the shading is ± 1 SEM.

(D) Quantification of the voltage signals. Left: peak $\Delta F/F$. Middle: t_{peak} . Right: full width at half maximum. The mean ± 1 SEM is plotted.

(E) Quantification of the calcium signals. * $p < 0.05$, ** $p < 0.01$, *** $p < 0.001$ (two-sample t test for peak $\Delta F/F$ and full width at half maximum, Mann-Whitney U test for t_{peak} ; Bonferroni correction for multiple comparisons).

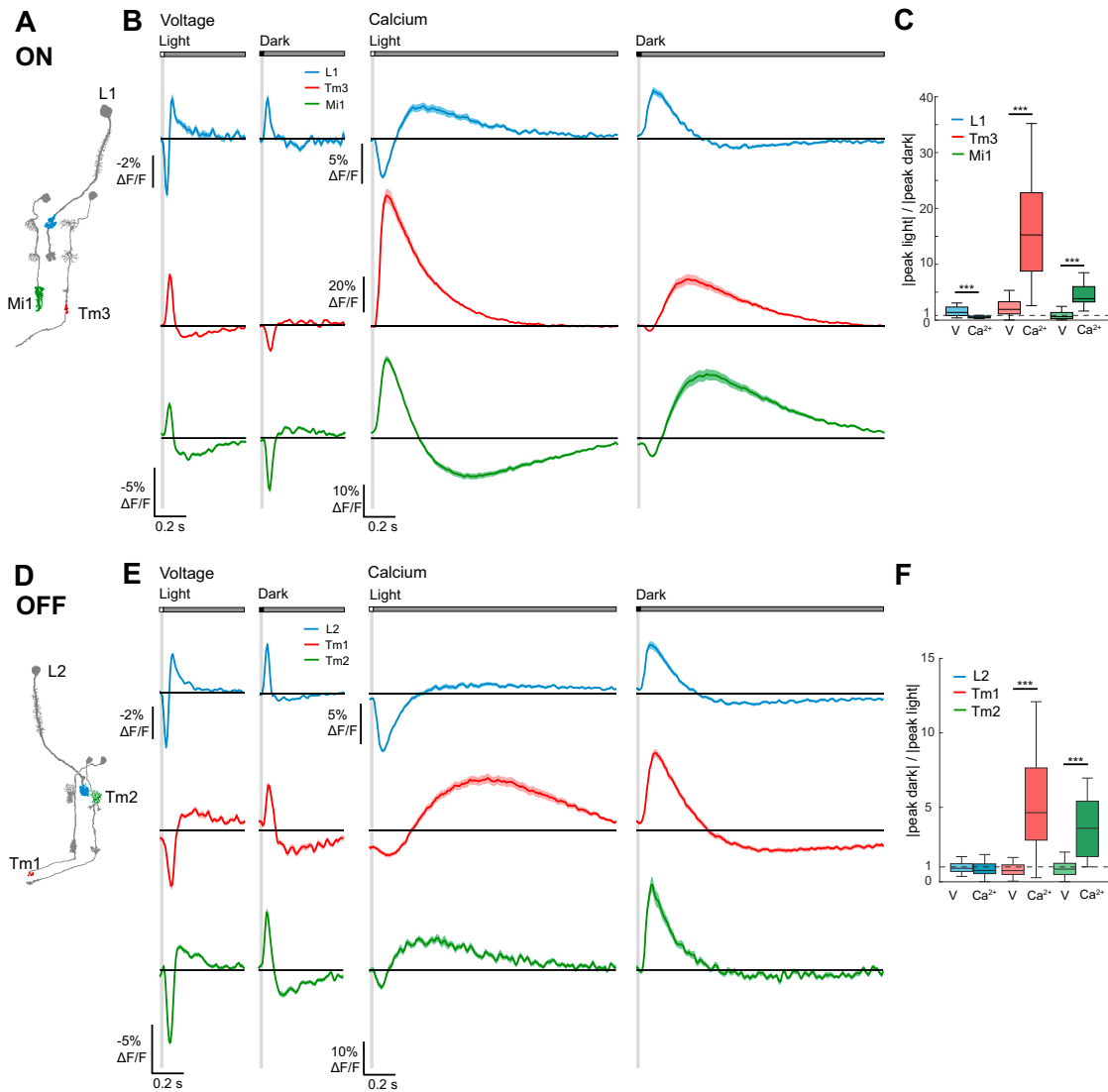


Figure S5. Contrast Selectivity of All ON and OFF Pathway Neurons, Related to Figures 6 and 7

(A) Illustration of the ON pathway with the imaged regions highlighted.

(B) Voltage responses (left) and calcium responses (right) of L1 layer M1 (blue; voltage: $n = 23$ cells, 6 flies and calcium: 42 cells, 4 flies), Tm3 layer M10 (red; voltage: $n = 100$ cells, 9 flies and calcium: $n = 99$ cells, 4 flies), and Mi1 layer M10 (green; voltage: $n = 67$ cells, 4 flies and calcium: $n = 89$ cells, 5 flies) to 25 ms light and dark flashes off of gray, contrast = 0.5. The solid line is the mean response; the shading is ± 1 SEM.

(C) Quantification of selectivity to light (ON). The line, box, and whiskers are the median, interquartile range, and maximum and minimum values within one interquartile range, respectively.

(D) Illustration of the OFF pathway with the imaged regions in L2, Tm1, and Tm2 highlighted.

(E) Voltage responses (left) and calcium responses (right) of L2 layer M2 (blue; voltage: $n = 125$ cells, 11 flies and calcium: 78 cells, 6 flies), Tm1 layer Lo1 (red; voltage: $n = 30$ cells, 3 flies and calcium: $n = 127$ cells, 9 flies), and Tm2 layer M2 (green; voltage: $n = 89$ cells, 6 flies and calcium: $n = 30$ cells, 6 flies).

(F) Quantification of selectivity to dark (OFF). *** $p < 0.001$ (Mann-Whitney U test, Bonferroni correction for multiple comparisons).

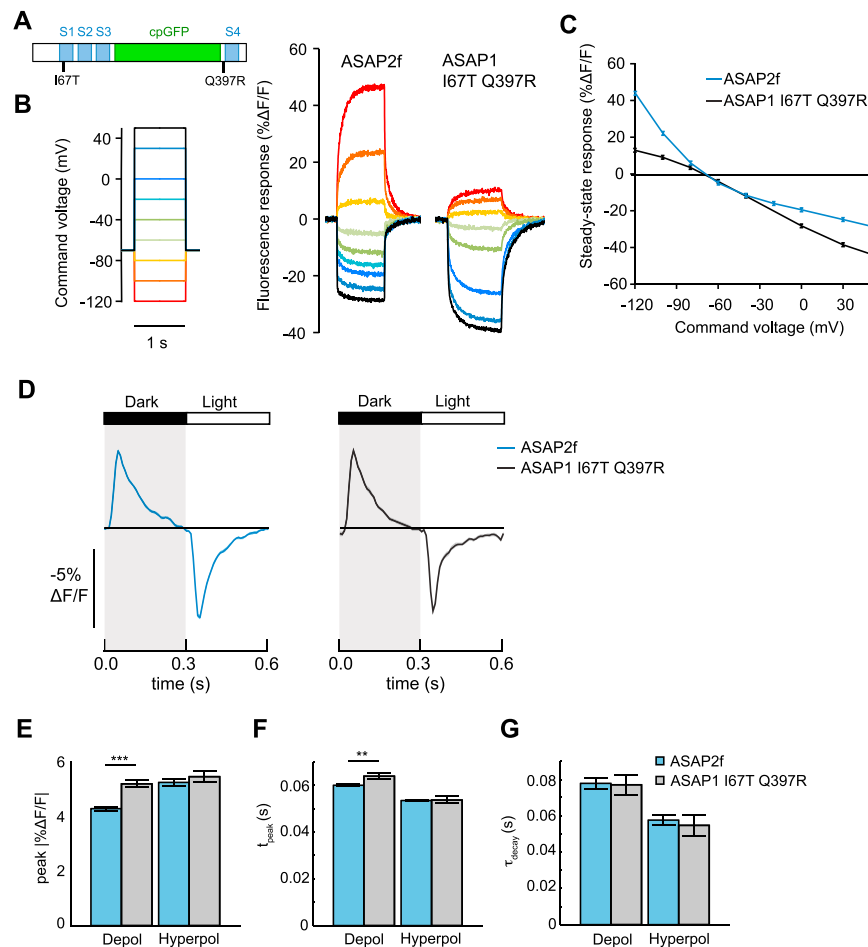


Figure S6. ASAP1 I67T Q397R Design and Characterization, Related to Figures 6 and 7

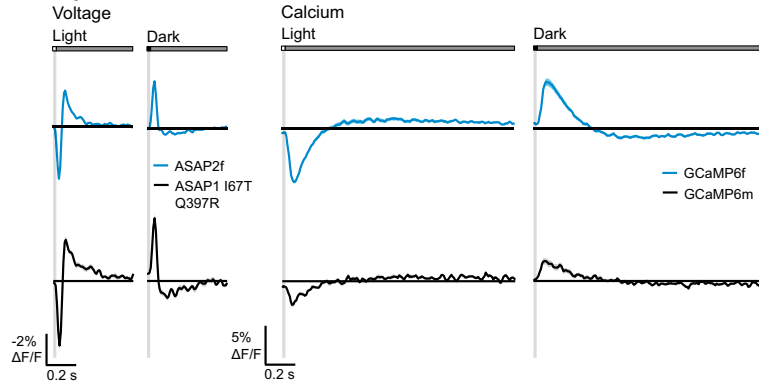
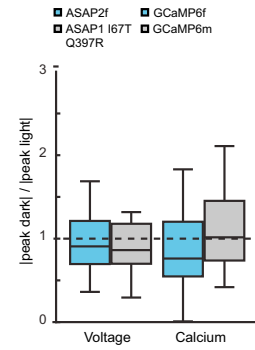
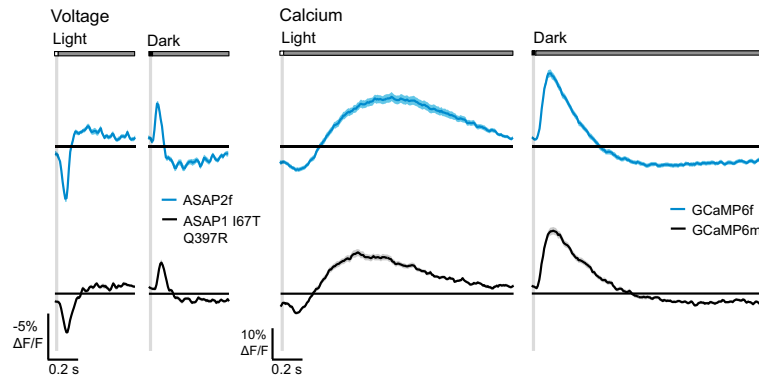
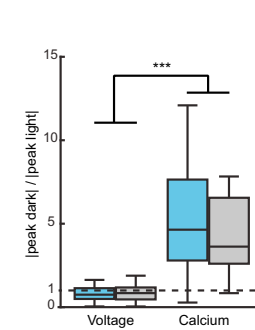
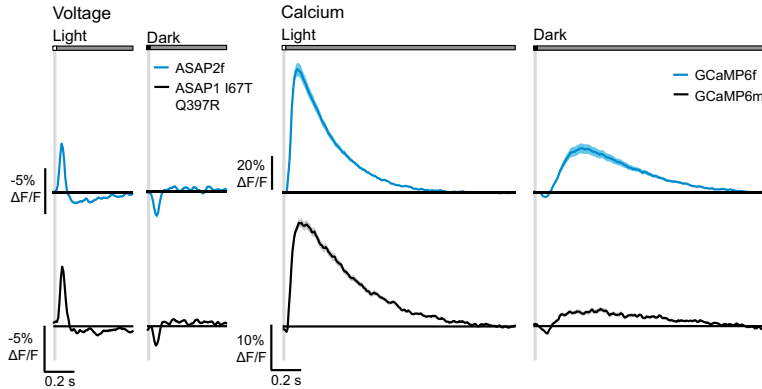
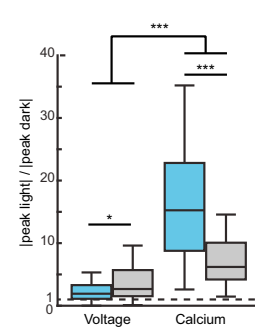
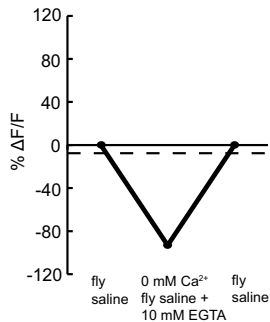
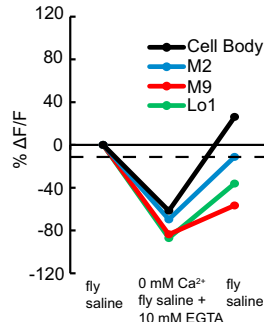
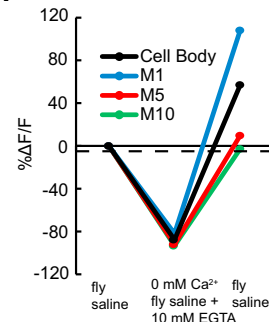
(A) Schematic diagram of ASAP1 I67T Q397R, showing the VSD transmembrane domains (S1-S4, blue), cpGFP, and the location of the new mutations I67T and Q397R.

(B) Representative fluorescence responses of ASAP2f and ASAP1 I67T Q397R to voltage steps from -120 to 50 mV in HEK293A cells. Responses were measured at 5-ms intervals and were normalized to the fluorescence at the -70 mV holding potential.

(C) Mean fluorescence response to transmembrane voltage of ASAP2f (n = 6) and ASAP1 I67T Q397R (n = 3).

(D) Responses of L2 neurons to alternating 300-ms dark and light flashes, as measured with ASAP2f (blue, n = 170 cells, 8 flies) and ASAP1 I67T Q397R (black, n = 94 cells, 5 flies).

(E-G) Parameters quantifying the response to alternating 300-ms dark and light flashes: (E) peak $\Delta F/F$, (F) t_{peak} , and (G) τ_{decay} . The mean \pm 1 SEM is plotted. **p < 0.01, ***p < 0.001 (two-sample t test, Bonferroni correction for multiple comparisons).

A L2 Layer M2**B****C Tm1 Layer Lo1****D****E Tm3 Layer M10****F****G L2****H Tm1****I Tm3**

(legend on next page)

Figure S7. Indicator Nonlinearities Do Not Underlie ON and OFF Selectivity, Related to Figures 6 and 7

(A–F) Voltage responses measured with ASAP1 I67T Q397R and calcium measured with GCaMP6m to 25 ms light and dark flashes off of gray, contrast 0.5. (A, B) L2 layer M2. $n = 125$ cells, 11 flies (ASAP2f); $n = 22$ cells, 2 flies (ASAP1 I67T Q397R); $n = 78$ cells, 6 flies (GCaMP6f); $n = 20$ cells, 3 flies (GCaMP6m). (C, D) Tm1 layer Lo1. $n = 30$ cells, 3 flies (ASAP2f); $n = 52$ cells, 5 flies (ASAP1 I67T Q397R); $n = 127$ cells, 9 flies (GCaMP6f); $n = 49$ cells, 3 flies (GCaMP6m). (E, F) Tm3 layer M10. $n = 100$ cells, 9 flies (ASAP2f); $n = 90$ cells, 5 flies (ASAP1 I67T Q397R); $n = 99$ cells, 4 flies (GCaMP6f); $n = 99$ cells, 5 flies (GCaMP6m). (A, C, E). Voltage (left) and calcium (right) response traces. The solid line is the mean response; the shading is ± 1 SEM (B, D). Quantification of selectivity to dark (OFF). (F) Quantification of selectivity to light (ON). The line, box, and whiskers are the median, interquartile range, and maximum and minimum values within one interquartile range, respectively. * $p < 0.05$, *** $p < 0.001$ (Mann-Whitney U test, Bonferroni correction for multiple comparisons).

(G–I) The change in GCaMP6f fluorescence when 0 mM Ca^{2+} and 10 mM EGTA fly saline was perfused to remove Ca^{2+} . The baseline fluorescence is the initial fluorescence in standard fly saline. (G) L2 layer M2. (H) Various compartments of Tm1. (I) Various compartments of Tm3. The dotted line indicates the minimum $\Delta F/F$ value evoked by visual stimulation of that cell.

Cell, Volume 166

Supplemental Information

Subcellular Imaging of Voltage and Calcium

Signals Reveals Neural Processing In Vivo

Helen H. Yang, François St-Pierre, Xulu Sun, Xiaozhe Ding, Michael Z. Lin, and Thomas R. Clandinin

SUPPLEMENTAL INFORMATION

SUPPLEMENTAL EXPERIMENTAL PROCEDURES

Plasmid construction for *in vitro* experiments. Plasmids were constructed by standard molecular biology methods and verified by sequencing of all cloned fragments. All ASAP variants were cloned between the NheI and HindIII sites of pcDNA3.1/Puro-CAG (Lam et al., 2012) and contain identical Kozak sequences. Expression plasmids and complete sequences for ASAP1, ASAP2f, and ASAP1 I67T Q397R can be obtained via Addgene.

HEK293A cell culture, patch clamping, and voltage imaging. HEK293A cells were maintained in high-glucose Dulbecco's Modified Eagle Medium (DMEM, HyClone) supplemented with 5% fetal bovine serum (FBS, Life Technologies) and 2 mM glutamine (Sigma) at 37 °C in air with 5% CO₂. Cells were plated onto glass-bottom 24-well plates (In vitro Scientific) for standard imaging or onto uncoated no. 0 12-mm coverslips (Glaswarenfabrik Karl Hecht GmbH) for patch clamping experiments. Transfections were carried out using FuGene HD (Promega) according to manufacturer instructions, except that cells were transfected at ~50% confluence with lower amounts of DNA (200 ng) and transfection reagent (0.6 µl) to reduce cell toxicity.

At 2 days post-transfection, cells were patch-clamped at 22 °C using borosilicate glass electrodes with resistances of 3.5 to 5.0 MΩ attached to an Axopatch 700B amplifier (Axon Instruments). Cells were superfused in a chamber mounted on the stage of an Axiovert 100M inverted microscope with a 40X/1.3-numerical aperture (NA) oil-immersion objective (Zeiss). The extracellular solution contained 110 mM NaCl, 26 mM sucrose, 23 mM glucose, 5 mM HEPES-Na, 5 mM KCl, 2.5 mM CaCl₂, and 1.3 mM MgSO₄, adjusted to pH 7.4. The intracellular (pipette) solution contained 115 mM potassium gluconate, 10 mM HEPES-Na, 10 mM EGTA, 10 mM glucose, 8 mM KCl, 5 mM MgCl₂, and 1 mM CaCl₂, adjusted to pH 7.4. Cells were illuminated with a high-power light-emitting diode (LED, UHP-MIC-LED-460, Prymatix) through a 470/30-nm filter at a power density of 3.7 to 23.7 mW/mm² at the sample plane. Fluorescence traces were acquired while cells were voltage clamped in whole-cell mode, using an iXon 860 electron multiplying charge coupled device camera (Andor) cooled to -80 °C and set to Frame Transfer mode. Fluorescence traces were corrected for photobleaching. Voltage and fluorescence traces were analyzed using custom software written in MATLAB (Mathworks). Voltage traces were corrected for the junction potential post hoc.

Unless otherwise indicated, step voltage depolarizations were applied to change the membrane potential from a holding voltage of -70 mV to voltages ranging from -120 mV to 50 mV for 1.0 s. For these voltage step experiments, we captured images at 200 Hz without binning, and the fluorescence response was measured from pixels at the perimeter of the cell (plasma membrane). For experiments with artificial action potential waveforms, we captured images at 1 kHz with 4 × 4 binning. The action potential waveform, derived from a recording of a hippocampal neuron action potential, had a full width at half maximum of 4.0 ms and peak amplitude of 100 mV. The fluorescence response was measured from the perimeter of the cell (plasma membrane). For experiments to determine sensor response kinetics, we increased sampling frame rate to 2.5 kHz by cropping the imaged area down to 64 × 64 pixels and increasing binning to 8 × 8 pixels. The resulting image thus contained 64 pixels (8 × 8); fluorescence was calculated by summing all 64 pixels. Command voltage steps were applied for 1 second; three identical voltage steps were measured for every cell. Models of the form $a \cdot e^{-bt} + c \cdot e^{-dt}$ were applied to the rising and falling portions of the mean fluorescence trace using MATLAB.

Quantifying voltage sensor brightness and photostability in HEK293 cells. For quantifying the brightness of ASAP variants, we used a HEK293 cell line expressing the inwardly rectifying Kir2.1 channel (Zhang et al., 2009) (HEK293-Kir2.1). This cell line, a generous gift of Gui-Rong Li, has a resting membrane potential of approximately -75mV, similar to that of primary hippocampal neurons. Cells were plated onto 60 mm tissue culture dishes at a density of 400,000 cells/dish. Cells were transfected using 3.6 µL of FuGENE HD reagent (Promega) and 1.2 µg of DNA per dish. At 2 days post-transfection, cells were collected by trypsinization using a 0.25% trypsin/EDTA solution (Gibco, Life Technologies), washed with phosphate buffered saline (PBS; HyClone, Life Technologies), and resuspended using a solution of Hank's Buffered Saline Solution (HyClone, Life Technologies) supplemented with 1% w/v bovine serum albumin and 5 mM ethylenediaminetetraacetic acid (EDTA). Cells were analyzed by flow cytometry using an LSRII.UV analyzer (BD Biosciences), using the 488-nm and 561-nm lasers to excite our GFP-based sensor and our FusionRed reference RFP, respectively. Gating conditions were set using Flowjo to analyze cells expressing ASAP-FusionRed constructs. We quantified the brightness of each cell as the ratio of green

fluorescence (from ASAP) and red fluorescence (from our FusionRed standard). The overall brightness of each construct was defined as the median brightness over all sensor-expressing cells.

For quantifying the photostability of ASAP variants, we transfected HEK293A or HEK293-Kir2.1 cells as previously described (St-Pierre et al., 2014). At 2 days post-transfection, cells were superfused with the same extracellular solution we used for electrophysiological recordings in HEK293A cells. To evaluate photostability under one-photon excitation, cells were imaged using an Axiovert 100M microscope (Zeiss) fitted with a 40X 1.3-NA oil-immersion objective (Zeiss). To collect images, we used the software HCLImage (Hamamatsu) to drive an ORCA Flash4.0 V2 C11440-22CU (Hamamatsu) scientific CMOS camera set to 4×4 pixel binning and cooled to -10 °C. Cells were continuously illuminated with a high-power light-emitting diode (LED, UHP-MIC-LED-460, Pryzmatic) through a 470/30-nm filter. To evaluate photostability under two-photon excitation, we used an Ultima Multiphoton Microscopy System (Prairie Technologies) equipped with a 40X LUM Plan FI W/IR-2 0.8-NA objective (Olympus). Cells were illuminated using a Mai Tai HP Deep See Ti:sapphire laser (Spectra-Physics) tuned to 920 nm and set to a power level of 4.7 mW. Laser scanning was performed using galvanometric mirrors. Each image pixel was sampled at 2.23 Hz with a dwell time of 0.4 μ s. Emitted photons were filtered using a 525/50-nm filter (Chroma) and collected using a non-descanned multi-alkali photomultiplier tube (Hamamatsu). For both one-photon and two-photon photobleaching time series, fluorescence from the entire cell was used to compute optical traces.

Neuronal cell culture and transfection. Animal experiments were performed in accordance with the rules of the Stanford University Administrative Panel on Laboratory Animal Care. Primary hippocampal or cortical neurons were dissected from Sprague-Dawley rats on embryonic day 22 and digested with 0.03% trypsin (Sigma) in Dulbecco's Modified Eagle Media (DMEM, HyClone) for 20 min at 37 °C in air with 5% CO₂. Neurons were then dissociated by gentle trituration in Hanks' Balanced Salt Solution (HBSS, Life Technologies) and washed twice in HBSS. Neurons were plated at 3.5×10^4 cells cm⁻² on 12-mm no. 0 coverslips (Glaswarenfabrik Karl Hecht GmbH) within wells of 24-well plates. Prior to plating, each coverslip was pre-coated for 24 hours with > 300 -kDa poly-D-lysine (Sigma) in PBS and washed three times with distilled water. Neurons were cultured overnight at 37 °C in air with 5% CO₂ in Neurobasal with $1 \times$ B27 supplement (Life Technologies), 2 mM GlutaMAX (Life Technologies), and 10% FBS. The following day, 90% of the medium was replaced with identical medium without FBS. Cytosine β -D-arabinofuranoside (Sigma) was added to a final concentration of 2 μ M when glia reached $> 70\%$ confluence, typically around 5 days *in vitro* (DIV). At 7 DIV, 50% of the media was replaced with fresh media without serum. Neurons were transfected at 7 to 9 DIV using 0.5 to 0.75 μ L of Lipofectamine 2000 (Life Technologies) and 800 ng of total DNA per well of a 24-well plate. Given the strong promoter (CAG) driving indicator expression, the 800 ng of total DNA per well consisted of 400 ng of indicator expression plasmid and 400 ng of pNCS, an empty bacterial expression plasmid (Lam et al., 2012).

Confocal Imaging of Rat Cortical Neurons. Rat cortical neurons were transfected at 8 DIV and imaged 3-4 days post-transfection in HBSS supplemented with 10 mM HEPES pH 7.4, $1 \times$ B27, 2 mM GlutaMAX, and 1 mM sodium pyruvate on an IX81 microscope with a FluoView FV1000 laser-scanning confocal unit operated using the FV10-ASW v3.01 software (Olympus). Fluorescence excitation was delivered using a 488-nm argon laser model #GLG3135 (Showa Optonics) through a 40X/1.3-NA oil-immersion objective (Olympus). Emission was passed through a 530/40-nm emission filter. Z-sections were imaged using a 1-Airy pinhole setting. A maximum-intensity projection was generated from 2-3 sections spaced 2 μ m apart.

Patch clamping and voltage imaging of dissociated neurons. At 11 to 13 DIV (2 to 4 days post-transfection), cultured neurons were patch-clamped at 22 °C using borosilicate glass electrodes with resistances of 3.5 to 5.0 M Ω attached to an Axopatch 700B amplifier (Axon Instruments). Cells were superfused in a chamber mounted on the stage of an Axiovert 100M inverted microscope with a 40X/1.3-NA oil-immersion objective (Zeiss). The extracellular solution contained 110 mM NaCl, 11 mM glucose, 5 mM HEPES-Na, 5 mM KCl, 2.5 mM CaCl₂, and 1.3 mM MgSO₄, adjusted to pH 7.4. The intracellular (pipette) solution contained 92 mM potassium gluconate, 8 mM HEPES-Na, 8 mM EGTA, 8 mM glucose, 6.4 mM KCl, 4 mM MgCl₂, and 0.8 mM CaCl₂, adjusted to pH 7.4. Cells were illuminated with a high-power light-emitting diode (UHP-MIC-LED-460, Pryzmatic) through a 470/30-nm filter at a power density of 23.7 mW/mm² at the sample plane. Images were captured at 1000 Hz with 4×4 binning using an iXon 860 electron multiplying charge coupled device camera (Andor) cooled to -80 °C in frame transfer mode. Fluorescence response was measured in all pixels from the cell body. Fluorescence traces were acquired while cells were current-clamped in whole-cell mode. For all experiments, fluorescence traces were corrected for photobleaching. To generate action potentials, 700 to 1100 pA of current was injected for 1 ms.

Analyzed neurons had the following characteristics: an access resistance less than 15 M Ω , a membrane resistance greater than 10 times the access resistance, and action potentials with peak height > 0 mV and width < 5 ms at -20 mV. Electrode voltages were recorded using pClamp (Axon Instruments). Voltage and fluorescence traces were analyzed using custom software written in MATLAB. Voltage traces were corrected for the junction potential post hoc.

Statistical methods for *in vitro* experiments. Results presented in the form $x \pm y$ represent the mean \pm SEM (standard error of the mean), unless indicated otherwise. Statistical comparisons of pre-identified measures of interest between two data sets were performed with the Student's t-test unless otherwise indicated. Prior to performing such statistical comparisons, the Shapiro-Wilk method was used to test the null hypothesis that the data followed a Gaussian (normal) distribution. When this normality hypothesis could not be rejected, Student's t-tests were performed; otherwise, the Mann-Whitney U nonparametric test was used. Prior to performing t-tests, we also tested the null hypothesis of equal variance between the two data sets, and employed Welch's correction when the null hypothesis was rejected. Statistical tests of normality and equal variance were performed with a significance level (α) of 0.05. When analyzing the results of a specific performance test, we applied the Bonferroni correction to the significance levels if more than one pairwise comparison was calculated. Statistical tests were performed in Excel (Microsoft) and MATLAB.

Transgenic Flies. The ASAP variants were cloned into the pJFRC7-20XUAS vector (Pfeiffer et al., 2010) using standard molecular biology methods to generate the *UAS-ASAP1*, *UAS-ASAP2f*, and *UAS-ASAP1 I67T Q397R* transgenes and inserted into the attP40 phiC31 landing site by injection of fertilized embryos (Rainbow Transgenic Flies, Inc.). *UAS-ASAP2f* was additionally inserted into the VK00005 phiC31 landing site though all experiments presented here used the attP40 insertion. GCaMP6f and GCaMP6m were expressed using *UAS-GCaMP6f* and *UAS-GCaMP6m* also inserted into attP40 (Chen et al., 2013). The L1 Gal4 driver (*R48A08AD*; *R66A01DBD*) was from Tuthill et al., 2013. The L2 Gal4 driver (*21D-Gal4*) was from Rister et al., 2007. The Mi1, Tm3, and Tm1 Gal4 drivers (*R19F01-Gal4*, *R13E12-Gal4*, and *R74G01-Gal4*, respectively) were from the Janelia FlyLight Project (<https://www.janelia.org/project-team/flylight>). The Tm2 Gal4 driver (*otd-Gal4*) was a generous gift from C. Desplan. The genotypes of the imaged flies were:

L1>>ASAP2f: w or +/+; *UAS-ASAP2f/R48A08AD*; *R66A01DBD/+*
L1>>GCaMP6f: w or +/+; *UAS-GCaMP6f/R48A08AD*; *R66A01DBD/+*
L2>>ASAP1: w/+; *UAS-ASAP1/+*; *21D-Gal4/+*
L2>>ASAP2f: w or +/+; *UAS-ASAP2f/+*; *21D-Gal4/+*
L2>>ASAP1 I67T Q397R: w or +/+; *UAS-ASAP1 I67T Q397R/+*; *21D-Gal4/+*
L2>>GCaMP6f: +/+; *UAS-GCaMP6f/+*; *21D-Gal4/+*
L2>>GCaMP6m: w/+; *UAS-GCaMP6m/+*; *21D-Gal4/+*
Mi1>>ASAP2f: w/+; *UAS-ASAP2f/+*; *R19F01-Gal4/+*
Mi1>>GCaMP6f: +/+; *UAS-GCaMP6f/+*; *R19F01-Gal4/+*
Tm3>>ASAP2f: w or +/+; *UAS-ASAP2f/+*; *R13E12-Gal4/+*
Tm3>>ASAP1 I67T Q397R: +/+; *UAS-ASAP1 I67T Q397R/+*; *R13E12-Gal4/+*
Tm3>>GCaMP6f: +/+; *UAS-GCaMP6f/+*; *R13E12-Gal4/+*
Tm3>>GCaMP6m: w/+; *UAS-GCaMP6m/+*; *R13E12-Gal4/+*
Tm1>>ASAP2f: w or +/+; *UAS-ASAP2f/+*; *R74G01-Gal4/+*
Tm1>>ASAP1 I67T Q397R: +/+; *UAS-ASAP1 I67T Q397R/+*; *R74G01-Gal4/+*
Tm1>>GCaMP6f: +/+; *UAS-GCaMP6f/+*; *R74G01-Gal4/+*
Tm1>>GCaMP6m: w/+; *UAS-GCaMP6m/+*; *R74G01-Gal4/+*
Tm2>>ASAP2f: w/+; *UAS-ASAP2f/GMR-Gal80*; *otd-Gal4/+*
Tm2>>GCaMP6f: +/+; *UAS-GCaMP6f/GMR-Gal80*; *otd-Gal4/+*

Fly Husbandry. All flies used for imaging were raised on standard molasses food at 25 °C on a 12/12-h light-dark cycle. Female flies of the appropriate genotypes were collected on CO₂ within 1 day of eclosion and imaged at room temperature (20°C) 5-6 days after eclosion. Tm2>>ASAP2f and Tm2>>GCaMP6f female flies were collected on ice within 1 day of eclosion and imaged the same day.

***In Vivo*, Two-Photon Imaging.** Flies were cold anaesthetized, positioned in a fly-shaped hole cut in steel foil such that their heads were tilted forward approximately 60° to expose the back of the head capsule above the foil while leaving most of the retina below the foil, and then affixed in place with UV-cured glue (NOA 68T from Norland

Products Inc.). The brain was exposed by removing the overlying cuticle and fat bodies with fine forceps, and an oxygenated saline-sugar solution (Wilson et al., 2004) was perfused over the fly. The saline composition was as follows: 103 mM NaCl, 3 mM KCl, 5 mM TES, 1 mM NaH₂PO₄, 4 mM MgCl₂, 1.5 mM CaCl₂, 10 mM trehalose, 10 mM glucose, 7 mM sucrose, and 26 mM NaHCO₃. The pH of the saline equilibrated near 7.3 when bubbled with 95% O₂/5% CO₂. Neurons were imaged with a Leica TCS SP5 II two-photon microscope with a Leica HCX APO 20X/1.0-NA water immersion objective (Leica) and a pre-compensated Chameleon Vision II femtosecond laser (Coherent, Inc.). The excitation wavelength was 920 nm and 5-15 mW of power was applied at the sample. Emitted photons were collected with a 525/50-nm filter. All data were acquired at a constant frame rate of 38.9 Hz using a frame size of 200×20 pixels, 15X digital zoom, a line scan rate of 1400 Hz, and bidirectional scanning. Imaging time per fly never exceeded 1.5 h.

Visual stimulation. Visual stimuli were generated with custom-written software using C++ and OpenGL and presented using a digital light projector as described previously (Clark et al., 2011). The visual stimulus was projected onto a coherent fiber optic bundle that then re-projected onto a rear-projection screen positioned approximately 4 cm anterior to the fly that spanned 80° of the fly's visual field horizontally and 50° vertically. Immediately prior to being projected onto the screen, the stimulus was filtered with a 447/60-nm bandpass filter so that it could not be detected by the microscope PMTs. The stimulus was refreshed at 240 Hz and had a radiance of approximately 30 mW·sr⁻¹·m⁻². The imaging and the visual stimulus presentation were synchronized as described in Freifeld et al., 2013. Following this procedure, the time of stimulus onset relative to the start of imaging varied within one stimulus frame (8.33 ms). To compensate for this, the average delay was measured (6.25 ms), and all imaging data was shifted in time by this delay.

The visual stimuli used were:

300 ms full field flash (Figures 1, S2, and S6): alternating full contrast light and dark flashes, each 300 ms in duration, were presented over the entire screen. This stimulus was presented for 2400 imaging frames (62 s) per field of view except in Figure S2 where 24000 imaging frames were presented (617 s).

8 ms light and dark flashes (Figure 2): single 8.33 ms light and dark flashes, with 500 ms of gray between the flashes, were presented over the entire screen. The light and dark flashes were alternated with each presentation. The Michelson contrast of the flashes relative to the gray was 0.5. This stimulus was presented for 4400 imaging frames (113 s) per field of view.

25 ms light and dark flashes (Figures 2-7, S3-S5, and S7): for voltage imaging, this stimulus was identical to the 8 ms flashes, except the light and dark flashes were 25 ms in duration. For calcium imaging, the gray interleave was extended to 1500 ms to account for the slower kinetics, and the stimulus was instead presented for 6600 imaging frames (170 s). In Figures 6 and 7, flashes with Michelson contrasts of 0.5, 0.25, and 0.125 were presented.

In vivo imaging data analysis. Raw images in each time series were aligned in x and y coordinates in ImageJ (NIH) using a macro based on the plugin Turboreg (<http://bigwww.epfl.ch/thevenaz/turboreg/>) and then further processed in MATLAB. Regions of interest (ROIs) around individual arbors or cell bodies were manually selected in the time series-averaged image. An example of such an image is shown in Figure 1E. For each imaging frame within the time series, intensity values for the pixels within each ROI were averaged and the mean background value (the average intensity in a region of the image without cells) was subtracted. To correct for bleaching, the time series for each ROI was fit with the sum of two exponentials, and in the calculation of $\Delta F/F = (F(t) - F_0)/F_0$, the fitted value at each time t was used as F_0 . For the 300 ms full field flash stimulus, all imaging frames were used to compute the fit, thereby placing $\Delta F/F = 0$ at the mean response after correction for bleaching. For the 8 or 25 ms light and dark flashes off of gray stimulus, only imaging frames that fell in the last 25% of the gray period were used to fit the bleaching curve; this places $\Delta F/F = 0$ at the mean baseline the cell returns to after responding to the flash instead of at the mean of the entire trace, which is inaccurate when the responses to the light and dark flashes are not equal and opposite. The stimulus-locked average was computed for each ROI by reassigning the timing of each imaging frame to be relative to the stimulus transitions (dark to light or light to dark for the 300 ms full field flash, gray to light or gray to dark for the flashes off of gray) and then computing a simple moving average with a 25 ms averaging window and a shift of 8.33 ms. This effectively resampled our data from 38.9 Hz to 120 Hz with 3-point boxcar smoothing but did not otherwise distort the fluorescence signal. As the screen on which the stimulus was presented did not span the fly's entire visual field, only a subset of imaged ROIs were actually observing the stimulus (empirically, approximately 70%). For Figures 1-5, S2-S5, and S7, responding ROIs were identified as those whose responses at time-matched points during the 2 stimulus epochs (dark and light flashes for the 300 ms full field flash and light to gray and dark to gray for the flashes off of gray) were significantly different (t-test, $p < 0.01$) for at least 3 consecutive time points. All calls were examined manually and adjusted if necessary. For Figures 6 and 7, ROIs

were presented with the 300 ms full field flash stimulus in addition to 25 ms flashes off of gray of different contrasts; responding ROIs were identified solely through their 300 ms full field flash response. All traces, except the single ROI and single trial examples in Figures 1F and 1G, are presented as the mean \pm 1 SEM across all of the responding ROIs of the moving average response to all trials of each ROI. In Figures 1F and 1G, bottom, the moving-average response across all trials of single example ROIs (that are approximately in the 75th percentile for response amplitude for all ROIs of that indicator) was plotted as mean \pm 1 SEM, and 5 0.6-s single trial excerpts of the $\Delta F/F$ trace for the same ROIs was presented in the single cell examples (plotted at the imaging frame rate of 38.9 Hz).

The quantification metrics for each ROI were computed as follows:

For the responses to the 300 ms full field flash stimulus in Figures 1 and S6, the peak response (peak $\Delta F/F$) during each phase (depolarization and hyperpolarization) was the absolute value of the $\Delta F/F$ value farthest from zero in the expected direction of the response. The time to peak (t_{peak}) was the time at which this peak response occurred, relative to the start of the stimulus. The decay of the response from the peak was fit with a single exponential and the time constant of this fit was τ_{decay} . The mean across all responding ROIs \pm 1 SEM was plotted, except for τ_{decay} , for which the ROIs were further filtered by those whose exponential decay fits had r values greater than 0.5. Pairwise Student's t-tests were performed, and multiple comparisons were corrected for using the Bonferroni method.

For the responses to the 25 ms light and dark flashes off of gray stimuli in Figures 3-5, S3, and S4, the peak response to each flash (peak $\Delta F/F$) was the $\Delta F/F$ value farthest from zero in the expected direction of the initial response (depolarization or hyperpolarization). The time to peak (t_{peak}) was the time at which this peak response occurred, relative to the start of the light or dark flash. The full width at half maximum was computed by identifying, for the rising phase of the response prior to t_{peak} and for the falling phase after t_{peak} , the two adjacent time points with $\Delta F/F$ values bracketing one-half of the peak $\Delta F/F$ value; fitting a line between two points to derive the time at which the value would be one-half of the peak $\Delta F/F$ value; and subtracting this time for the rising phase from that of the falling phase. Some traces were too noisy to identify the two adjacent time points with $\Delta F/F$ values bracketing one-half of the peak $\Delta F/F$ value; such traces were excluded. In Figures 4 and S3, pairwise Student's t-tests were performed for the peak $\Delta F/F$ and full width at half maximum metrics, and the Mann-Whitney U test was performed for the t_{peak} metric. Multiple comparisons were corrected for using the Bonferroni method. In Figures 5 and S4, one-way ANOVAs were performed for the peak $\Delta F/F$ and full width at half maximum metrics and followed by post-hoc pairwise t-tests with the Bonferroni correction for multiple comparisons; the Kruskal-Wallis test followed by post-hoc pairwise Mann-Whitney U tests with the Bonferroni correction for multiple comparisons were performed for the t_{peak} metric.

For Figure 3C, the fraction decay from M1 was computed as the mean peak $\Delta F/F$ of the indicated region divided by the mean peak $\Delta F/F$ of layer M1. The error bars were computed as $\text{mean}_{\text{fraction decay}} \times (\text{SEM}_{\text{region}}/\text{mean}_{\text{region}} + \text{SEM}_{\text{M1}}/\text{mean}_{\text{M1}})$.

For Figures 6, 7, S5, and S7, the stimulus was 25 ms light and dark flashes off of gray, and selectivity for ON and OFF was computed as: $|\text{peak light response}/\text{peak dark response}|$ for the ON pathway and $|\text{peak dark response}/\text{peak light response}|$ for the OFF pathway. The peak response was quantified as the maximal $\Delta F/F$ of the initial response phase minus the average $\Delta F/F$ value before the response. For Figure 7, the index was computed separately for each of the 3 pairs of contrast values. When the response is perfectly linear, this index equals 1. Selectivity was computed for each individual ROI, and a box and whisker plot across ROIs was plotted for each condition. The line indicates the median, the box indicates the interquartile range, the whiskers extend to the maximum or minimum values less than one interquartile range past the box, and outliers are omitted. Mann-Whitney U tests with the Bonferroni correction for multiple comparisons were performed.

NEURON modeling (Figures 3E-3H). The morphology of Mi1 from the Janelia Fly EM: Medulla TEM Reconstruction project (Takemura et al., 2013) was downloaded from the Chklovskii Archive in the Neuromorpho public repository. The neuron used was the central column neuron Mi1 215. The .swc morphology was loaded into NEURON 7.4 (www.neuron.yale.edu; Carnevale and Hines, 2006) using the Import 3D tool and exported to the CellBuilder tool, which converted the morphology to a multi-compartment cell geometry for the model. To complete the cell, a single-segment cell body of diameter 5 μm and length 5 μm was attached to the end of the most distal process by a process of diameter 250 nm and length 10 μm . The model neuron was given uniform passive membrane properties, estimated from the parameters in (Behnia et al., 2014; Cuntz et al., 2013; Gouwens and Wilson, 2009; Haag et al., 1996): resting membrane potential = -70 mV, axial resistance = 40 to 420 $\Omega\cdot\text{cm}$, specific membrane capacitance = 1 $\mu\text{F}/\text{cm}^2$, and specific membrane resistance = 1 to 21 $\text{k}\Omega\cdot\text{cm}^2$. 50 pA of current was injected into layer M1 for 20 ms. The duration of the simulation was 100 ms. The membrane potential responses over time were recorded in the arbors of layers M1, M5, and M10. The peak membrane potential measured during

current injection was determined and heat maps were generated displaying the fraction of this peak membrane potential relative to that achieved in layer M1. This was compared to the decays ± 1 SEM measured with ASAP2f imaging.

GCaMP6f dynamic range analysis (Figures S7G-S7I). To determine the maximal decrease in fluorescence GCaMP6f is capable of achieving *in vivo*, we imaged while first flowing in the standard oxygenated fly saline (for 2 min), then flowing in a modified oxygenated fly saline with 0 mM CaCl_2 and 10 mM EGTA (for 10 min), and then flowing in standard oxygenated fly saline (for 10 min). The entire extent of the medulla and lobula was imaged simultaneously. Data was acquired at 1 Hz, using an imaging window of 512×300 px, 3X digital zoom, a line scan rate of 400 Hz, and bidirectional scanning. These time series were processed identically to those measuring visually evoked responses, except as subsequently described. ROIs were manually drawn around the terminals and cell bodies, with one ROI for each layer. $\Delta F/F$ was computed using the mean fluorescence during the initial standard saline epoch as the baseline F_0 . The mean $\Delta F/F$ during each solution epoch was computed by averaging $\Delta F/F$ over the frames during which the fluorescence had stabilized, chosen manually for each time series but consistent among ROIs from the same time series. The minimum $\Delta F/F$ achievable was therefore -100%.

	ASAP1	ASAP2f
<i>Depol. (–70 to 30 mV)</i>		
τ_{fast} (ms)	2.9 ± 0.3	2.8 ± 0.1
τ_{slow} (ms)	161 ± 33	135 ± 16
% fast	74 ± 5	81 ± 2
<i>Repol. (30 to –70 mV)</i>		
τ_{fast} (ms)	2.3 ± 0.4	2.4 ± 0.2
τ_{slow} (ms)	177 ± 38	155 ± 16
% fast	63 ± 6	71 ± 3
<i>Hyperpol. (–70 to –100 mV)</i>		
τ_{fast} (ms)	11 ± 3	8.8 ± 1.0
τ_{slow} (ms)	131 ± 16	142 ± 15
% fast	59 ± 3	54 ± 4
<i>Repol. (–100 to –70 mV)</i>		
τ_{fast} (ms)	15 ± 3	13 ± 1
τ_{slow} (ms)	131 ± 14	154 ± 9
% fast	52 ± 2	50 ± 4

n = 4–5 cells per sensor. Data are presented as mean \pm SEM.

Table S1. Related to Figure 1. Response kinetics of ASAP indicators in HEK293A cells.

SUPPLEMENTAL REFERENCES

Freifeld, L., Clark, D.A., Schnitzer, M.J., Horowitz, M.A., and Clandinin, T.R. (2013). GABAergic Lateral Interactions Tune the Early Stages of Visual Processing in *Drosophila*. *Neuron* 78, 1075–1089.

Lam, A.J., St-Pierre, F., Gong, Y., Marshall, J.D., Cranfill, P.J., Baird, M.A., McKeown, M.R., Wiedenmann, J., Davidson, M.W., Schnitzer, M.J., et al. (2012). Improving FRET dynamic range with bright green and red fluorescent proteins. *Nat. Methods* 9, 1005–1012.

Pfeiffer, B.D., Ngo, T.-T.B., Hibbard, K.L., Murphy, C., Jenett, A., Truman, J.W., and Rubin, G.M. (2010). Refinement of Tools for Targeted Gene Expression in *Drosophila*. *Genetics* 186, 735–755.

Rister, J., Pauls, D., Schnell, B., Ting, C.-Y., Lee, C.-H., Sinakevitch, I., Morante, J., Strausfeld, N.J., Ito, K., and Heisenberg, M. (2007). Dissection of the Peripheral Motion Channel in the Visual System of *Drosophila melanogaster*. *Neuron* 56, 155–170.

Tuthill, J.C., Nern, A., Holtz, S.L., Rubin, G.M., and Reiser, M.B. (2013). Contributions of the 12 Neuron Classes in the Fly Lamina to Motion Vision. *Neuron* 79, 128–140.

Wilson, R.I., Turner, G.C., and Laurent, G. (2004). Transformation of olfactory representations in the *Drosophila* antennal lobe. *Science* 303, 366–370.

Zhang, D.-Y., Lau, C.-P., and Li, G.-R. (2009). Human Kir2.1 channel carries a transient outward potassium current with inward rectification. *Pflugers Arch.* 457, 1275–1285.